UNIVERSITÀ DEGLI STUDI DELLA TUSCIA DI VITERBO

Dipartimento di Scienze dell'Ambiente Forestale e delle sue Risorse

The emissions of greenhouse gases from forest fires in the Mediterranean Region

Tesi di Dottorato

Ilaria Palumbo

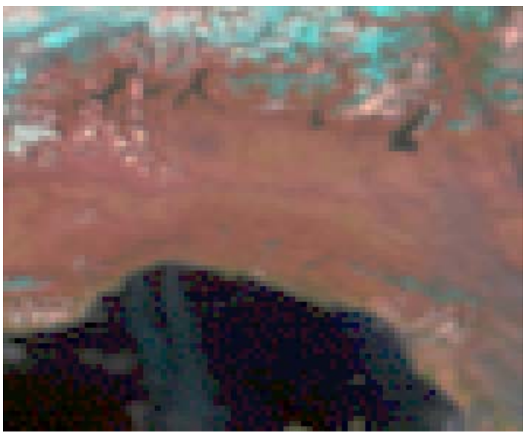

2007

UNIVERSITÀ DEGLI STUDI DELLA TUSCIA DI VITERBO

Dipartimento di Scienze dell'Ambiente Forestale e delle sue Risorse

CORSO DI DOTTORATO DI RICERCA

ECOLOGIA FORESTALE XIX CICLO

The emissions of greenhouse gases from forest fires in the Mediterranean Region

AGR/05

Coordinatore: Prof. Paolo de Angelis

Firma

Tutori: Prof. Riccardo Valentini e Dott. Paulo Barbosa

Firma

Dottoranda: Ilaria Palumbo

Firma

Table of Contents

Abstract

Forest fires occur regularly in the Mediterranean Basin affecting several hundred thousands hectares every year. Most of fires, about 90% of the total, are human-induced.

A relevant effect of this burning activity is the emission of greenhouse gases which has been recognised as an important issue by the United Nations Framework Convention on Climate Change (UNFCCC) and the Kyoto Protocol. Although it is crucial to have reliable information about the fire emissions, current estimates are still affected by high uncertainties mostly due to the inaccuracy of the data used in the analysis.

The major contribution to the level of uncertainty is given by the information about the burned biomass. Therefore in this study a recent method for the estimation of the burned biomass is applied by using satellite remote sensing.

The original approach has been developed in the tropical region and is based on the radiant energy emitted during the burning of vegetation (Fire Radiative Power, FRP). It has been shown that the FRP is linearly related to the amount of burned biomass.

This research activity provides for the first time provides an assessment of the FRP in the forest fires of a Mediterranean ecosystem. The original method is therefore implemented to become applicable in this specific environment. The analysis has been carried out on three case studies by using the satellite imagery from the SEVIRI (Spinning Enhanced Visible and Infra-Red Imager) geostationary sensor on board the Meteosat Second Generation platform.

A fire detection algorithm has been developed by applying a multispectral approach which uses the mid (3-5 μm) and thermal (10-12 μm) infrared bands. The identification of actve fires is essential for the application of the FRP method. The emitted energy is derived for each active fire during its whole duration so that the total radiant energy emitted is quantified (Fire Radiative Energy, FRE). The amount of burned biomass is estimated from the FRE by using the relation derived from previous studies carried out in the tropical area. It is assumed that the equation is also valid for the Mediterranean ecosystems since it is independent of the vegetation type.

In addition to the satellite analysis the assessment has been integrated with field data collected from the study sites. The information from the field has been used to evaluate the accuracy of the estimates of burned biomass derived from the FRE.

The results showed the feasibility of using the SEVIRI sensor for fire monitoring despite its low spatial resolution. The comparison of the FRE estimates with those derived from the field showed good agreement. Differences vary between 36% and 3% indicating a lower uncertainty when compared to that of the current methods used

to estimate burned biomass. This result demonstrates that the FRP approach is applicable in the Mediterranean region and thus providing significant improvements in the estimates of fire emissions in its ecosystems.

The GHG emissions have been quantified by using the burned biomass estimates derived from the FRE and from the field data. Their amounts can influence substantially the effects of air pollution on human health at local scale and can also contribute to climate change on a broader scale.

Riassunto

Nel bacino del Mediterraneo centinaia di migliaia di ettari vengono bruciati ogni anno con cause diverse, ma nel 90% dei casi come conseguenza dell'azione dell'uomo.

Tra gli effetti del fuoco le emissioni gassose rivestono un ruolo fondamentale come già riconosciuto dalla Convenzione sui Cambiamenti Climatici (UNFCCC) e dal Protocollo di Kyoto. Pertanto è diventato fondamentale poter quantificare in modo accurato le emissioni di gas serra rilasciate negli incendi boschivi. Tuttavia le attuali stime sulle emissioni presentano un'ampia incertezza dovuta principalmente alla scarsa accuratezza dei dati impiegati nell'analisi.

La variabile che apporta il maggior contributo di incertezza alle stime sulle emissioni è la biomassa vegetale bruciata. Pertanto in questo lavoro di ricerca si propone l'applicazione di un metodo di recente sviluppo per derivare le informazioni sulla biomassa bruciata utilizzando il telerilevamento satellitare.

Il metodo originale è stato sviluppato in ambiente tropicale e si basa sulla misura dell'energia radiante emessa durante l'incendio (Fire Radiative Power, FRP), poiché è stato dimostrato che questa energia è legata in modo lineare alla quantità di biomassa bruciata.

L'attività di ricerca qui presentata studia per la prima volta l'FRP in incendi boschivi dell'ecosistema mediterraneo e pertanto la metodologia originaria è stata implementata per renderla applicabile a questo specifico ambiente. L'analisi è stata svolta su tre casi studio utilizzando le immagini acquisite dal sensore geostazionario SEVIRI (Spinning Enhanced Visible and Infra-Red Imager) a bordo del satellite Meteosat Second Generation.

Prima di tutto è stato sviluppato un algoritmo per il riconoscimento degli incendi attivi utilizzando diverse bande spettrali tra cui l'infrarosso medio (3-5 μm) e termico (10-12 μm). L'identificazione degli incendi attivi è essenziale ai fini dell'applicazione della metodologia FRP. L'energia emessa è derivata su ciascun incendio attivo e per l'intera durata dell'incendio. In questo modo l'energia radiante emessa complessivamente (Fire Radiative Energy, FRE) viene determinata. La quantità di biomassa combusta viene stimata a partire dall'FRE utilizzando una relazione derivata da precedenti lavori svolti in area tropicale. L'equazione per la conversione dell'FRE in biomassa bruciata è considerata valida anche per la vegetazione mediterranea in quanto la relazione risulta essere indipendente dal tipo di vegetazione considerata.

Oltre all'analisi satellitare sono anche state svolte delle campagne di misure a terra finalizzate alla raccolta di dati sulla biomassa bruciata nei casi studio analizzati. Questi dati sono stati impiegati per valutare l'accuratezza delle stime di biomassa bruciata derivate dall'FRE.

I risultati dello studio dimostrano la funzionalità del sensore SEVIRI ai fini del monitoraggio degli incendi boschivi, pur avendo una bassa risoluzione spaziale. Nel confronto tra le stime della biomassa bruciata derivata dall'energia emessa (FRE) con quelle ottenute dai rilievi di campo si osserva un buon accordo: le differenze variano tra il 36% ed il 3%. Tali differenze indicano un livello di incertezza di molto inferiore a quello che attualmente caratterizza le stime di biomassa bruciata e dimostrano come il metodo FRP sia applicabile all'ambiente mediterraneo e come questo approccio possa significativamente migliorare le attuali stime delle emissioni rilasciate dagli incendi boschivi.

Le emissioni di gas serra sono state quantificate a partire dai valori di biomassa bruciata derivati dall'FRE e dai dati di campo. Le quantità emesse risultano significative sia per gli effetti che hanno sull'inquinamento atmosferico, e quindi sulla salute delle persone, sia per il contributo che possono apportare ai cambiamenti climatici.

List of Figures

List of Tables

List of Acronyms

ATSR Along Track Scanning Radiometer

AVHRR Advanced Very High Resolution Radiometer

BRF Bidirectional Reflectance Factor

CFS Corpo Forestale dello Stato

SRTM Shuttle Radar Topography Mission

EFFIS European Forest Fires Information System

EOS Earth Observing System

ESDB European Soil Database

EXPRESSO Experiment for Regional Sources and Sinks Of Oxidants

FAO Food and Agriculture Organization of the United Nations

FIRESCAN Fire Research Campaign Asia-North

FRE Fire Radiative Energy

FRP Fire Radiative Power

HRV High Resolution Visible

ISAFA Istituto Sperimentale per l'Assestamento Forestale e per l'Alpicoltura

LULUCF Land Use, Land-use Change and Forestry

MAS MODIS Airborne Simulator

MIR Mid-Infrared

MODIS Moderate Resolution Imaging Spectro-radiometer

MSG Meteosat Second Generation

NOAA National Oceanic and Atmospheric Administration

PAH polycyclic aromatic hydrocarbons

SAFARI-92 (Southern African Fire-Atmosphere Research Initiative

SCAR-B Smoke, Clouds and Radiation in Brazil

SCAR-C Smoke, Clouds and Radiation in California

SEVIRI Spinning Enhanced Visible and Infra-Red Imager

TIR Thermal-Infrared

TRACE-A Transport and Atmospheric Chemistry near the Equator-Atlantic

UNFCCC United Nations Framework Convention on Climate Change

VOC volatile organic compounds

WRB World Reference Base for Soil Resources

Introduction

Research context

Biomass burning is a relevant phenomenon which impacts every component of the biosphere. It affects the world's vegetation including forests, savannas and agricultural areas. According to the inventories from the FAO several millions hectares of forests are burned every year affecting an area covering 0.9 percent of the global forested areas (FAO, 2001). In addition to such an amount, fire burns large areas of other wooded lands.

If we consider the Mediterranean Basin fire activity regularly affects several hundred thousands hectares (European Commission, 2006) with consequences on ecosystems and local air pollution. Although fire has serious impacts on human health and the environment, the information about the amount of vegetation affected and the related fire emissions is still very poor.

Burning is used for clearing of lands, land conversion, agriculture and domestic use. Fire has an important ecological role: it shapes and maintains natural ecosystems, it has several positive impacts on vegetation renovation and, as a disturbance, it can even favour biodiversity (Goudsblom, 1992).

Besides its benefits fire is also a destructive factor for the environment. It can accelerate erosion processes and land degradation, it destroys vegetation communities and, in many cases, it is a danger for human life. Biomass burning releases a significant amount of gases and particulates which have a relevant impact on the atmospheric chemistry and air pollution, radiation budget and climate (Levine et al., 1995). Since the 1980s emissions from vegetation fires have been recognized as an important issue to assess because the amount of some atmospheric pollutants turned to be comparable to that from the fossil fuel combustion. Compared to annual global emissions from anthropogenic sources biomass burning contributes up to 40% and 38% of gross carbon dioxide and tropospheric ozone respectively (Seiler and Crutzen, 1980; Crutzen and Andreae, 1990, Levine, 1991). The assessment of the amounts of trace gases and particulates emitted from fires is therefore an important environmental issue. It also has political implications in the context of the UNFCCC (United Nations Framework Convention on Climate Change) and the Kyoto Protocol. This was also stated at the International Wildland Fire Summit in 2003 where the need for more accurate information about fire activity was pointed out: *"Informed policy and decision-making clearly requires timely quantification of fire activity and its impacts nationally, regionally and globally. Such information is currently largely unavailable"* (International Forest Fire News, IFFN No. 29).

In the last two decades many studies have been carried out to improve the understanding of the fire contribution to global gaseous emissions. Several international experiments (ground based, airborne and spaceborne observations) have been organized in order to collect data on fires such as the burned area, the smoke and trace gases emissions. These experiments mainly focused on tropical and boreal regions some of the more relevant are: SAFARI-92 (Southern African Fire-Atmosphere Research Initiative; Andreae et al., 1996, Lindesay et al., 1996), TRACE-A (Transport and Atmospheric Chemistry near the Equator-Atlantic; Fishman et al., 1996), over Brazil and the south Atlantic; SCAR-B (Smoke, Clouds and Radiation; Kaufman et al., 1998a, 1998b) over Brazil; EXPRESSO (Experiment for Regional Sources and Sinks Of Oxidants; Delmas et al., 1999) in central Africa; FIRESCAN (Fire Research Campaign Asia-North; FIRESCAN Science Team, 1996) in central Siberia, SAFARI 2000 (Queface et al, 2003; Elias et al. 2003; Anyamba et al., 2003; Swap et al., 2003; Manson et al., 2003; Drouin et al., 2003; Buermann et al., 2003).

According to Levine (1991) carbon released from fire activity can vary, globally, between 2000-5000 Tg every year. Such variability is not only due to natural reasons, but it is mostly related to the uncertainty in current emission estimates.

Current models combine information on the emission factors with the amount of burned biomass to provide this measure (Seiler and Crutzen, 1980). Emission factors are the amount of the chemical species released per mass of burned biomass; they have been determined in laboratories and field experiments and are now available for most of the gas species with an uncertainty of 20-30%,. On the other hand, burned biomass estimates show an uncertainty level of around 50% (Andreae and Merlet, 2001). Because of this, global emissions inventories are still affected by very high uncertainties (more than 50%) and improvements are needed.

Burned biomass has usually been determined considering the amount of fuel load available to burn and the related burning efficiency. These factors vary in time and space and therefore a real time assessment would be required. However, measuring the amount of fuel load and the related burning efficiency in real time is particularly difficult. Remote sensing is a powerful tool for such an objective and has been recently used to implement a new method. It is based on the radiant energy released by fires, the Fire Radiative Energy (FRE), that has been shown to be related to the amount of burned biomass (Kaufman et al., 1996, 1998a, 1998b). The relation between the radiant energy measured by spaceborne sensors and the amount of biomass consumed during burning has been assessed in several field experiments carried out in the tropical regions (Wooster et al., 2005; Roberts et al., 2005). Although the relation with burned biomass seems to be independent of the vegetation type, the application of the FRE is still relatively new and further work is necessary to implement the current method and assess its validity in non-tropical ecosystems.

Objectives of research work

The objectives of the present work aim at the implementation of the actual estimates of forest fire emissions in the Mediterranean Basin. They are described in details in the list below.

- The assessment of active fires.

This objective is carried out using the SEVIRI imagery (Spinning Enhanced Visible and Infra-Red Imager) onboard the Meteosat-8 platform. Although the SEVIRI instrument is not designed for fire monitoring purpose, its high temporal resolution (an image every 15 minutes) is of key importance for studying active fires during their life span. Moreover, the new spectral bands provide information in the mid and thermal infrared which is required for fire identification.

In order to monitor the fire events in an automatic way an algorithm for the detection of active fires is developed. This part of the research also contributes with new insights to the use of the SEVIRI imagery for fire monitoring application. The assessment of active fires is presented in Chapters 3 and 4 (Sections 3.1. and 4.1. respectively).

- The estimation of the amount of burned biomass using satellite remote sensing.

In order to fulfil this objective the FRE method is applied. The existing approach developed by Wooster et al. (2005) is used for the first time in a Mediterranean ecosystem, therefore the FRE method is implemented to adapt it to this specific environment. The assessment of the burned biomass with the satellite application is described in Chapters 3 and 4 (Sections 3.2. and 4.2. respectively). The analysis of active fires and FRE is carried out on selected wildfires which are considered as case studies.

- The preliminary validation of the FRE method using field data.

Besides the satellite applications, the study areas have been sampled in several field campaigns which were carried out to collect ground data of burned biomass. The availability of these measurements allows the first comparison between the amounts of burned biomass derived from the FRE with those provided by the field campaign. The results of the comparison are shown in Chapter 4 (Section 4.4.). This preliminary validation offers an important contribution to present understandings about the FRE application in the context of the fire emissions research.

- The estimation of gaseous emissions.

The emissions are estimated by using the burned biomass derived by the FRE. Results are also compared with emission estimates computed by using the burned biomass derived from the field data. This final objective is described in Chapters 3 and 4 (Section 3.4. and 4.5. respectively).

Structure of the thesis

The first chapter presents the forest fire dynamics and the remote sensing techniques used to assess them. Fire phenomenon is introduced as a global issue, but specific attention is dedicated to the Mediterranean ecosystem. In addition this section contains a review of past and present remote sensing methods used for the analysis of fires.

The second chapter describes the datasets and the satellite sensors used in the analysis; it also presents the case studies and the information collected during the field campaigns.

The third chapter presents the methods applied in the analysis: the fire detection algorithm, the FRE approach and the implementations made to adapt them to the Mediterranean ecosystem. Moreover it reports the methods used for the estimation of the burned biomass from the field measures and the emission factors used to derive the emissions released during the fire events.

In the fourth chapter the results about the fire detection and the FRE are reported and discussed. The burned biomass estimates derived from the FRE are compared with the field data in order to present a preliminary evaluation of the accuracy of the FRE application. The gaseous and the particulates species emitted during the combustion are also shown.

The conclusions of the study are outlined in the fifth chapter and finally the outlooks of the research activity are presented.

Chapter 1

1. Context of research

1.1. Biomass Burning in the Biosphere

1.1.1. Effects of fire on ecosystems and atmosphere

Fire is a common phenomenon occurring worldwide, from tropical to boreal regions. About 90% of all fires are human-induced; natural causes are lightning and self-combustion. Fire can be used as a land management tool in agricultural practices, land conversion and land clearing.

It affects different ecological processes: biotic and abiotic. It shapes landscape diversity and influences biogeochemical cycles, particularly the global carbon cycle. It can have many positive effects on ecosystems: it controls insect pests and has an important ecological role in the nutrient cycles. After burning many nutrients become available in the ash layer which is rich in phosphorus, potassium, calcium, and magnesium. In addition fire contributes to seed dispersal and high temperatures can stimulate seed germination.

On the other hand fire has detrimental effects if vegetation is not adapted to it. It can cause significant loss of biodiversity and it damages soil if combustion of the litter layer is intense. Once organic material is removed, soil becomes prone to the erosion process. Another relevant effect of biomass burning is the emission of gaseous compounds into the atmosphere. According to the International Forest Fire News (IFFN No. 29) several hundred million hectares of forest and other vegetation types are burned every year. Such activity can contribute up to one-fifth of the total global emissions of carbon dioxide (Levine and Cofer, 2000; Schimel, 1995).

The main chemical species released during fire activity are: carbon monoxide, methane, non-methane hydrocarbons, nitric oxide and methyl chloride with CO_2 and CO accounting for about 87% of the whole C-based emissions (Lobert et al., 1991). The species mentioned above have a greenhouse effect and contribute to global warming. The volatile organic compounds (VOCs), and the polycyclic aromatic hydrocarbons (PAHs) participate to photochemical reactions which lead to the production of tropospheric ozone. Aerosols (e.g. black carbon, particulate organic carbon) have an impact on the radiation budget since they can scatter or absorb the incoming solar radiation and hence impact the global climate.

Due to long-range transport in the atmosphere, fire emissions have impacts from local to global scale. Besides the direct release of trace gases, the burning of forests destroys important sinks for carbon dioxide and has a long-term effect with implications for the climate (Levine, 1991). Effects of fire on atmosphere and climate are shown in figure 1.1.

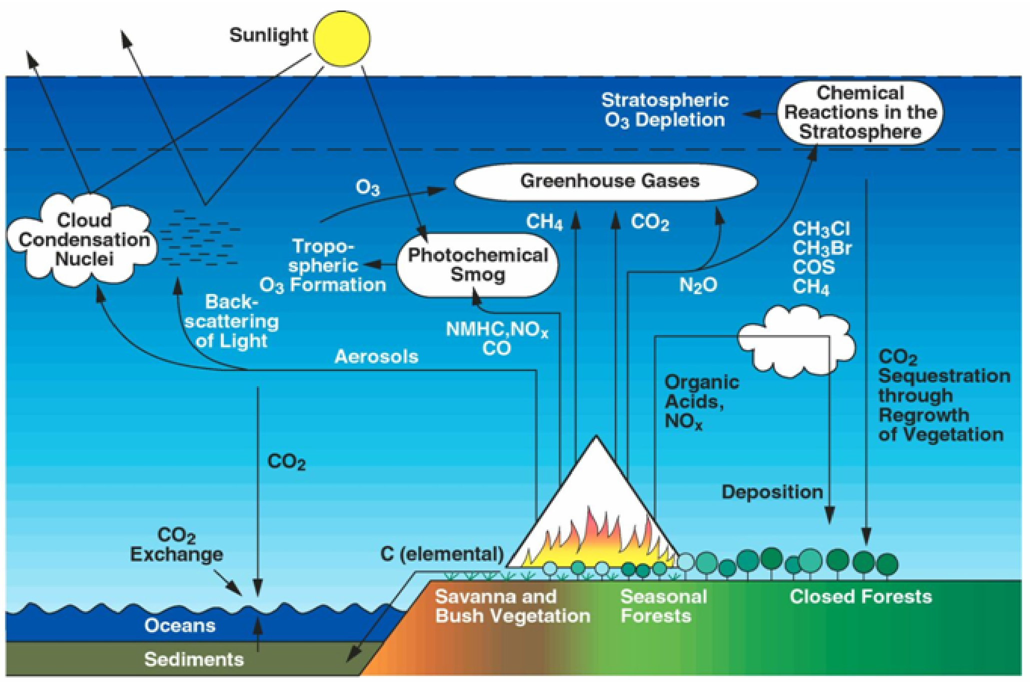

Source: Global Fire Monitoring Centre (GFMC).

Figure 1.1. The impact of gaseous and aerosols emissions from vegetation fires on atmosphere and climate

After the work by Seiler and Crutzen in 1980 biomass burning was finally recognized as a significant contributor to atmospheric greenhouse gases emissions. After their first assessment, many other studies followed confirming its relevance at global level (Crutzen and Andreae, 1990; Andreae, 1991; Levine, 1996).

According to Levine (1995) 8700 Tg of CO_2 are emitted every year with about 3500 Tg from biomass burning activity. Compared to all other sources of trace gases emissions biomass burning shows a significant contribution as reported in table 1.1.

Species	Biomass burning (Tg element/year)	All sources (Tg element/year)	Biomass burning (%)
CO_2 (gross)	3500	8700	40
CO_2 (net)	1800	7000	26
CO	350	1100	32
CH_4	38	380	10
NMHC	24	100	24
NO	8.5	40	21
NH_3	5.3	44	12
S	2.8	150	2
[a]O_3 (tropospheric)	420	1100	38
Total particulate matter	104	1530	7
Particulate organic carbon	69	180	39
Elementar carbon	19	<22	>86

[a]O_3 is not a direct product of biomass burning but results from photochemical reactions

Source: Levine et al., 1995.

Table 1.1. The contribution of biomass burning to global emissions from all sources.

1.1.2. The burning process

Vegetation biomass is made of cellulose and hemicelluloses (50–70% of dry matter), lignin (15–35%), proteins and amino acids. It also contains minerals (up to 10%) and water (up to 60%) and volatile substances such as alcohols, aldehydes, terpenes (Lobert and Warnatz, 1993). Although vegetation has a variability of compounds the carbon content is quite stable across different vegetation types. It is comprises between 45 and 50% of dry biomass weight (Schlesinger, 1991). Therefore, if the combustion of vegetation is complete, the result is carbon dioxide and water and can be simplified as follows:

$$(C_6H_{12}O_6)_n \rightarrow CO_2 + H_2O + 1.28*10^6 \text{ KJ} \quad (1)$$

However, in a real fire many other chemical species are produced, also depending on the chemical-physical phase which is occurring. Most of the chemical compounds released are carbon-based species like CO_2, CO, CH_4, NMHCs, CH_3Cl and NO_x, NH_3.

During the first phase, called *preignition*, fuel is dehydrated and *pyrolysis* occurs. Once fire is ignited pyrolysis continues as a first thermal process followed by *combustion*. These two processes can however be concurrent. Combustion includes *flaming, smoldering* and *glowing* (figure 1.2.). The final phase of a fire is *extinction*. Each phase has different chemical processes that result in different type of emissions.

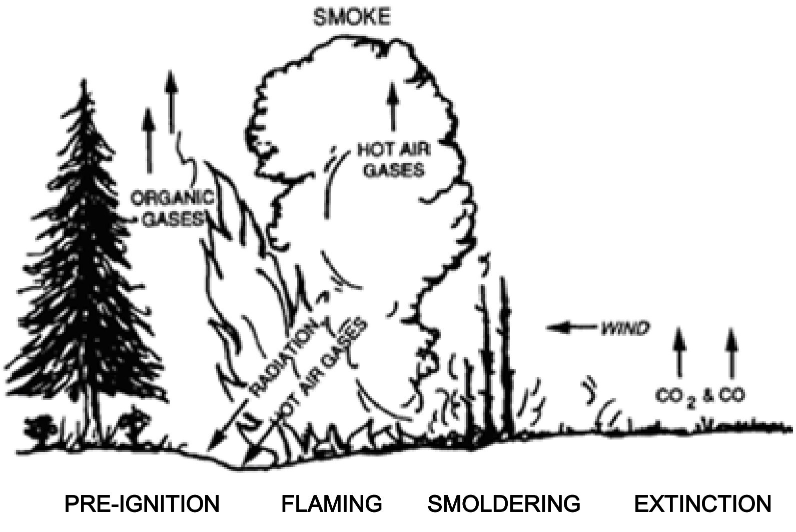

Source: DeBano et al., 1998

Figure 1.2. Phases of a fire

In order to ignite a fire, temperature has to be above 100°C, then water vapor and volatile organic extractives are distilled from the fuel into the air. *Pyrolysis* starts during this stage. Pyrolysis is an endothermic reaction which elevates fuel temperatures and degrades organic molecules of plant cells. Cellulose and hemicelluloses are the first compounds to be thermally decomposed. Their breakdown results in the production of tars, polymers, char, CO_2, CO, water vapour and highly flammable (high-molecular-weight) hydrocarbon vapours and gases. When temperature rises to 300-400°C fire becomes self-sustaining: the heat released during the reaction supplies the thermal energy needed to maintain pyrolysis and ignites more fuel. This second thermal process is exothermic. It determines the rapid oxidation of hydrocarbon vapors released from the fuel surface. Gas products mixed with air form a flammable combination which initiates the *flaming combustion*. In this phase the mixture of substances emitted during pyrolysis is converted into simple molecules like CO_2, H_2O, NO, N_2O, N_2 and SO_2, in addition intermediate products are also released: CO, CH_4, H_2, C_2H_4, C_2H_2, PAH and particles. During the flaming phase temperature can reach 1400°C and the oxidation reaction occurs in the gas phase. The heat produced accelerates the rate of pyrolysis and as a consequence releases a greater amount of flammable gases. When charcoal formation reduces the thermal conductivity of the fuel and the flux of heat decreases, *smoldering* combustion becomes dominant. The oxidation reaction occurs in the solid phase between oxygen and carbon from the char layer. The rate of fire spread is reduced because the fuel does not provide enough combustible gases. Atmospheric emissions (especially particulate products) are significantly greater than those from the flaming phase. Temperature is usually lower than 600°C during smoldering combustion. The final part of the smoldering process is named *glowing*. During this phase burning continues at the surface of the charred fuel. Little smoke is present and the main products released are CO, CO_2 and ash. This phase of burning shows high efficiency since it has a slow rate of combustion, with higher O_2 concentration. Maximum temperatures do not exceed 300-600°C. Finally fire gets to the *extinction* phase when all the available fuel is consumed or when the temperature is insufficient for fuel heating (DeBano et al., 1998).

1.1.3. Current estimates of fire emissions

In order to quantify the amount of trace gases released, current methods use the amount of burned biomass and the emission factor associated with the specific chemical species. The equation used has been first proposed by Seiler and Crutzen (1980). It is the following:

$$E(x) = M \times EF \qquad (2)$$

where

E(x) is the total amount of X-species released (grams),

M is the total amount of biomass burned (kg),

EF is the emission factor of the X-species (grams of X-species per kg of dry matter burned).

The amount of burned biomass and the emission factor depend on ecosystem, fire type and burning conditions.

Emission factors have been measured in many laboratory and field experiments now available for a large variety of species emitted in different ecosystems. The uncertainty associated to emission factors is around 20-30% (Andreae and Merlet 2001).

Burned biomass is usually derived combining information on burned areas, fuel load and combustion efficiency.

$$M = A \times B \times \alpha \times \beta \qquad (3)$$

where

A is the total land area burned,
B is the average biomass material per unit area (grams of dry material per m^2),
α is the fraction of the aboveground biomass relative to the total average biomass B,
β is the burning efficiency of the aboveground biomass.

The level of uncertainty attached to burned biomass is around 50% (Andreae and Merlet 2001). Whereas estimates of the burned area (A) are now available with improved accuracy from satellite remote sensing products. The main contribution to the final uncertainty comes from factors B, α and β.

Combustion efficiency (β) and fuel load (B) have been measured in some experimental fires all over the world, but there is still a lack of information especially on non tropical ecosystems (e.g. Mediterranean). Furthermore, due to their high variability in time and space, these variables require frequent updates which would be possible only using a remote sensing approach. Unfortunately it has been demonstrated that it is difficult to assess them through the current satellite remote sensing systems (French et al., 2004). Consequently burned biomass estimates are affected by large uncertainty which leading to wide error margins (more than 50%) in fire emissions inventories. Global burned biomass estimates for different ecosystems, from different authors, are reported in table 1.2. with the corresponding amount of carbon released. The data show a high level of variability among each ecosystem type and at global level. Moreover it can be noticed that there is no specific information for the Mediterranean ecosystem which is included in the general class termed *Temperate and Boreal forest*.

Source	Biomass Burned (Tg dm/year)				C released (Tg C/year)
	Seiler and Crutzen (1980)	Hao et al. (1990)	Andreae (1991)	Dignon[a]	
Tropical forest	2420	1260	1260	1230	550-1090
Savannas	1190	3690	3690	3470	540-1660
Temperate/boreal forest	280	-	280	520	130-230
Fuel wood	1050	620	1430	1880	280-850
Charcoal	-	-	21	-	30
Agricultural waste	1900	660	2020	1360	300-910
Tundra	-	-	-	4	2
World total	6840	6230	8700	7660	1800-4740

[a]Dignon and Penner (1991), Dignon (1988)

Table 1.2. Global burned biomass estimates and carbon released in different ecosystems from different authors.

Due to the limitations in the current approaches another methodology has been proposed to determine burned biomass. It uses the energy radiated during the burning process (Fire Radiative Energy, FRE), because this is related to the rate of combustion of vegetation and to the amount of chemical species released (Kaufman et al., 1996; Kaufman et al., 1998b). FRE can be measured from satellite sensors using the infrared spectral bands.

Once the fire energy is determined, burned biomass is derived using the empirical relation suggested by Wooster et al. 2005. In the present study the FRE methodology is implemented to be applied in the Mediterranean ecosystem.

1.1.4. Fire in the Mediterranean Basin

Fire is a recurrent phenomenon in the Mediterranean basin. The number of fire events and the total area affected have important consequences in terms of land degradation and air pollution. As with the global level, the main cause of fire is anthropogenic (around 95% of total), mostly due to deliberate lighting of forest fires and negligence. Agricultural practices are often responsible for unwanted wildfires. In addition the abandonment of countryside, caused by the migration of population to urban areas, has facilitated vegetation regrowth increasing the flammable fuel layer and the susceptibility to fire. Another factor contributing to fire risk is the rural mismanagement.

Fire is a characterizing feature of vegetation and landscape in the Mediterranean Basin. In this region vegetation is dominated by evergreen shrubs, woodlands with sclerophyllous and coniferous trees, and forests with evergreen trees. The more common species and plant genera are: *Quercus ilex, Quercus suber, Pinus pinaster, Pinus pinea, Pinus halepensis, Pinus nigra, Calluna sp., Arbutus unedo, Ceratonia sp., Larus sp., Erica sp., Cistus sp., Lavandula sp., Rosmarinus sp., Salvia sp., Olea sp., Phillyrea sp., Cedrus libani spp., Chamaerops sp., Buxus sempervirens.*

Usually we refer to Mediterranean shrubs as *Maquis* in case of dense shrub formations or *Garrigue* if vegetation is more open. Vegetation in the Mediterranean region is extremely rich, more than four times the number of floral species found in all the rest of Europe (IUCN and WWF).

Many types of vegetation have evolved with fire they are adaptated to it or even fire-dependent. Some examples of adaptation are the thick barks of trees (e.g. *Quercus suber*), the possibility of new shoots from the base roots (e.g. *Pistacia lentiscus, Arbutus unedo*) and the production of serotinous cones which can spread their seeds after a fire event (e.g. *Pinus halepensis*).

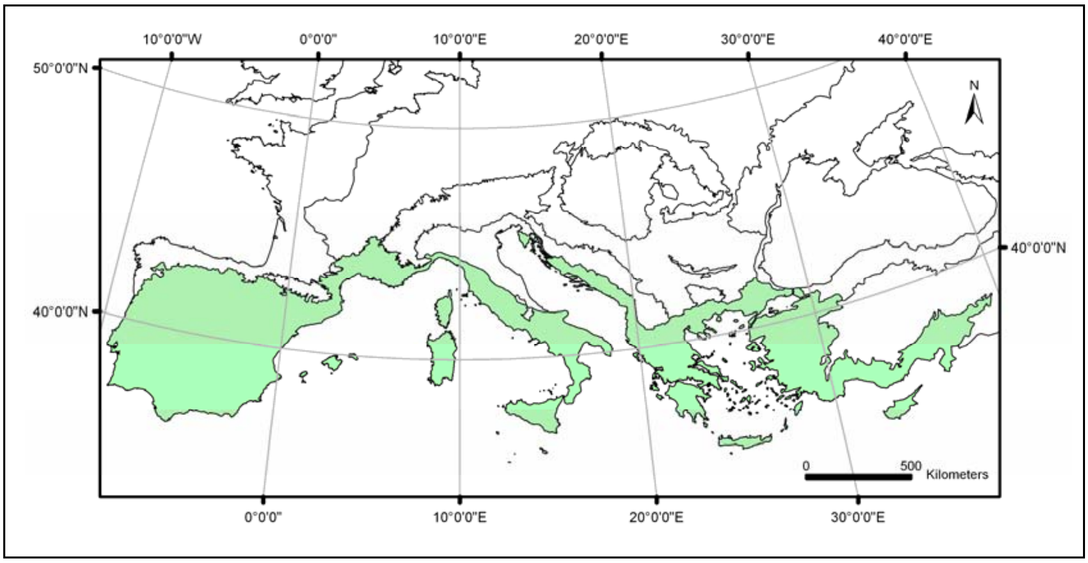

Figure 1.3. The Mediterranean Basin.

The Mediterranean climate is dominated by hot and dry summer with mild and wet winter. Because of favourable weather conditions most fires usually occur during summer with a typical peak in August. However some fires are also registered during the winter season when dry conditions and strong wind occur. This is especially the case for northern Italy. On average the fire return interval in the Mediterranean region is around 10-40 years (Mouillot et al., 2003). This period is valid for different types of vegetation with longer intervals typical of the forest ecosystems.

In order to deal effectively with the forest fire issue, the European Union has supported those Member States that undertook programmes for prevention, suppression of fires and restoration of fire affected areas since the Eighties. In addition in 1999 the European Commission, through its Directorate General Joint Research Centre (JRC), set up a research group with the specific objective of monitoring forest fire risk and mapping burned areas at European scale. Within this context in 2003 the European Forest Fires Information System (EFFIS, web page: http://effis.jrc.it/Home/) has been established at the Institute for Environment and Sustainability (IES) of the JRC. At present, EFFIS provides fire danger forecast and an implemented rapid damage assessment; it also includes an EU Fire Database with forest fire information from some of the Member States. At present 18 Member States of the Union are contributing to the Database the period of available data is indicated in brackets: Portugal (1985-2004), Spain (1985-2004), France (1985-2004), Greece (1985-2004), Italy (1994-2004), Germany (1994-2005), Poland (1993-2005), Sweden (1996-2004), Croatia (1996-2005), Cyprus (2000-2005), Hungary (2002-2005), Czech Republic (2004-2005), Latvia (2004-2005), Lithuania (2004), Slovakia (2004-2005), Romania (2004-2005), Finland (2005), Turkey (2005) (http://effis.jrc.it/EU_Fire_Database/). An example of fire risk map provided by EFFIS is shown in figure 1.4.

According to EFFIS several hundred thousands hectares are burned throughout European forests every year (http://effis.jrc.it/documents/2006/EFFIS_Newsletter-2006_02.pdf). The longer time series of data are available for Portugal, Spain, France, Italy and Greece which are also the more affected countries in Europe. Trends of fire activity in these Member States are reported in figures 1.5. and 1.6.

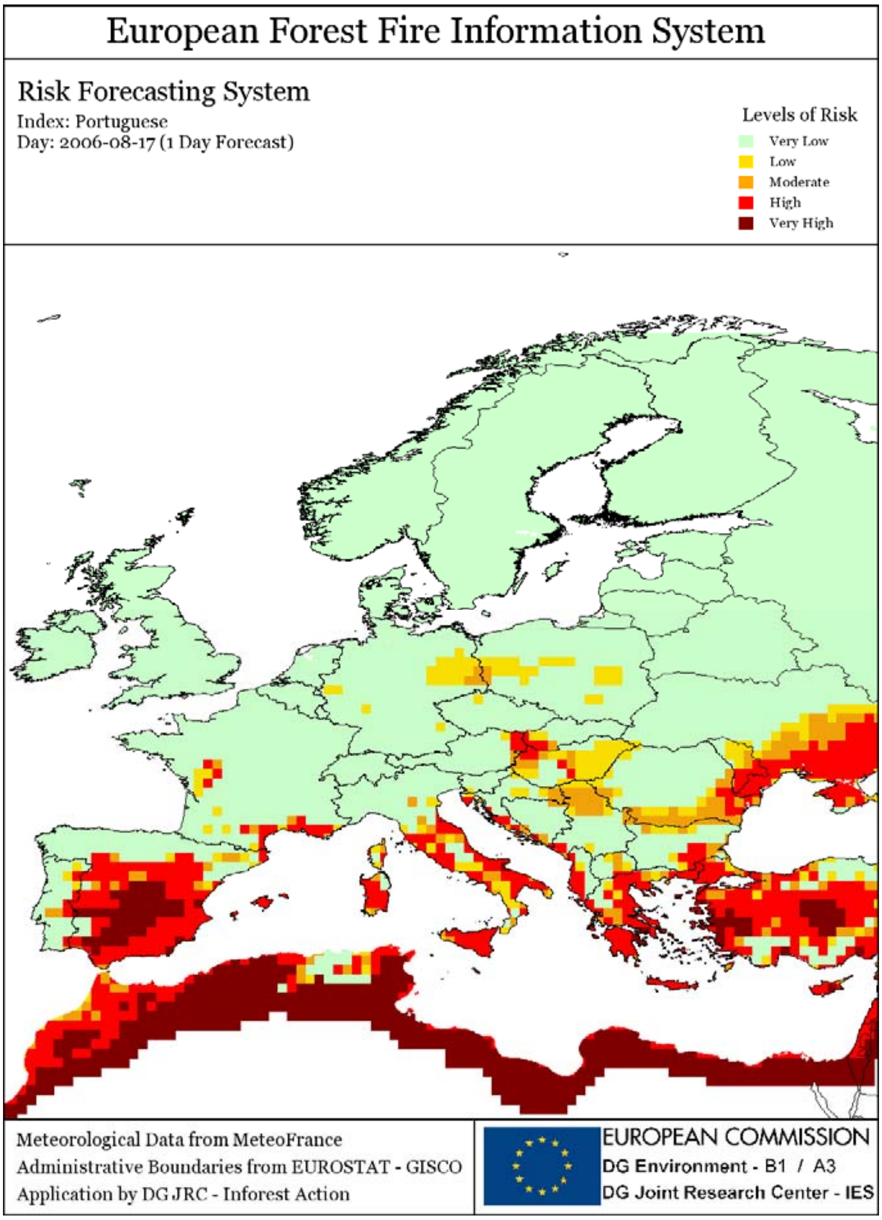

Source: EFFIS

Figure 1.4. Daily fire risk level estimated with the Fire Weather Index (FWI).

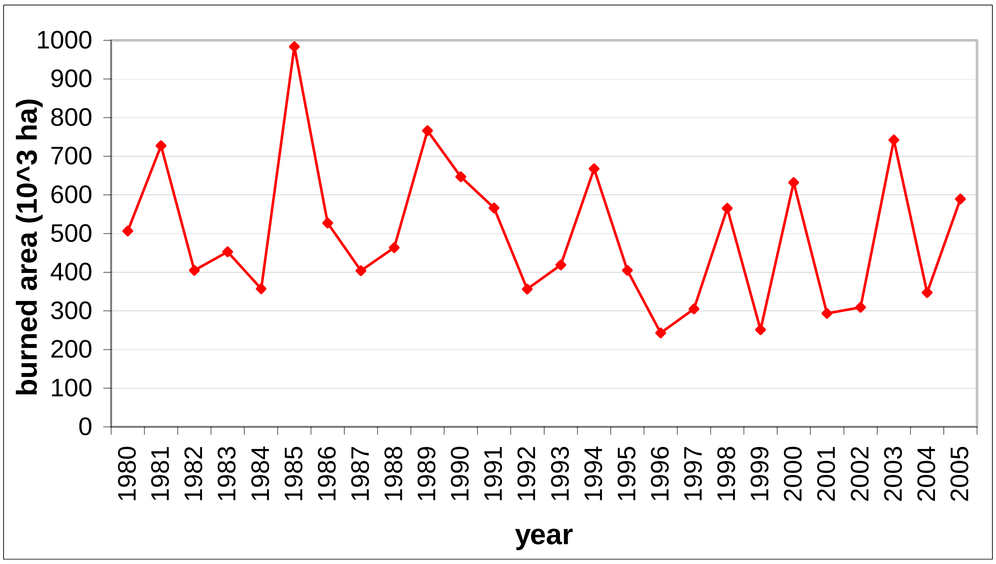

Figure1.5. Burned area in five Member States (Portugal, Spain, France, Italy and Greece)

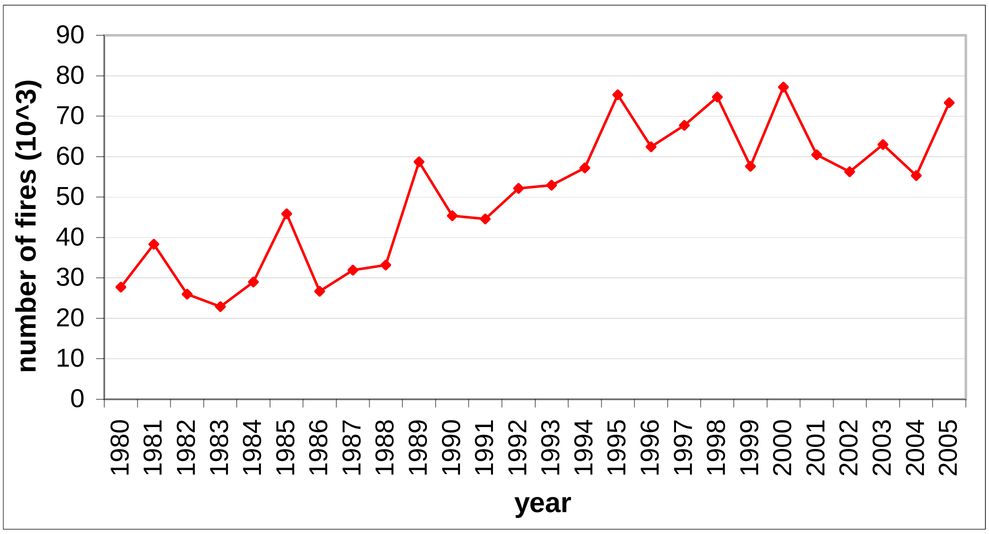

Figure 1.6. Number of fires in five Member States (Portugal, Spain, France, Italy and Greece)

A recent study observes an increase of fire risk in Spain during the period 1941-1994 concluding that global warming might cause an increase in the number of wildfires in this region (Piñol et al., 1998). Similar conclusions are drawn by a study on Portuguese forest fires (Miranda, 1994). Moreover the impact of fire activity is not negligible in terms of greenhouse gases emissions as showed in a recent UN report about Portuguese GHG inventories (FCCC/ARR/2005/PRT). Emissions from wildfires are accounted as part of LULUCF (Land Use, Land-use Change and Forestry) and become relevant for Kyoto Protocol commitments.

1.2. Remote Sensing of forest fires

Fire affects ecosystems worldwide and can impact large areas of landscape often located in remote regions. Due to these conditions ground monitoring of fire activity can be very time consuming and expensive in terms of resources involved. Therefore satellite remote sensing offers a unique opportunity for fire observation providing information at different spatial and temporal scales. The application of remote sensing techniques to study fire activity started in the 1990s (Robinson, 1991) using sensors which were not specifically designed for fire monitoring. One of the first applications used the AVHRR (Advanced Very High Resolution Radiometer) instrument, on-board NOAA (National Oceanic and Atmospheric Administration) platform, to identify active fires (Levine, 1996; Malingreau, 1990). Lately many other satellite sensors have been developed and our capability of fire characterization at global and regional level has been improved.

Vegetation fires show several spectral characteristics which are detectable by RS sensors. Fires can be identified while occurring by the presence of smoke and heat, whereas, once the active phase is over, fire occurrence is recognized by the burned scar left on the ground which contrasts with the non-affected vegetated landscape.

1.2.1. Active fires

Active fires are detectable because they show a typical thermal anomaly in the spectral signal which contrasts with that of the surrounding landscape. The spectral radiation of a body changes with its temperature and its emitted energy can be retrieved as a function of wavelength using the Plank function [$B(\lambda, T)$]. As shown in figure 1.7., objects at different temperatures have a peak of emitted energy at different wavelengths: the higher the temperature the shorter the wavelength where the maximum is reached.

Active fires have temperatures in the range 500-1000 K with a peak of energy emission in the region of 3-5 µm which corresponds to the often so-called mid-infrared domain (MIR). This spectral range is therefore very useful to identify active fires. Another spectral region with an important role for fire detection is the thermal infrared (TIR, 8-14 µm). Therefore the two channels are often used together for a more accurate assessment.

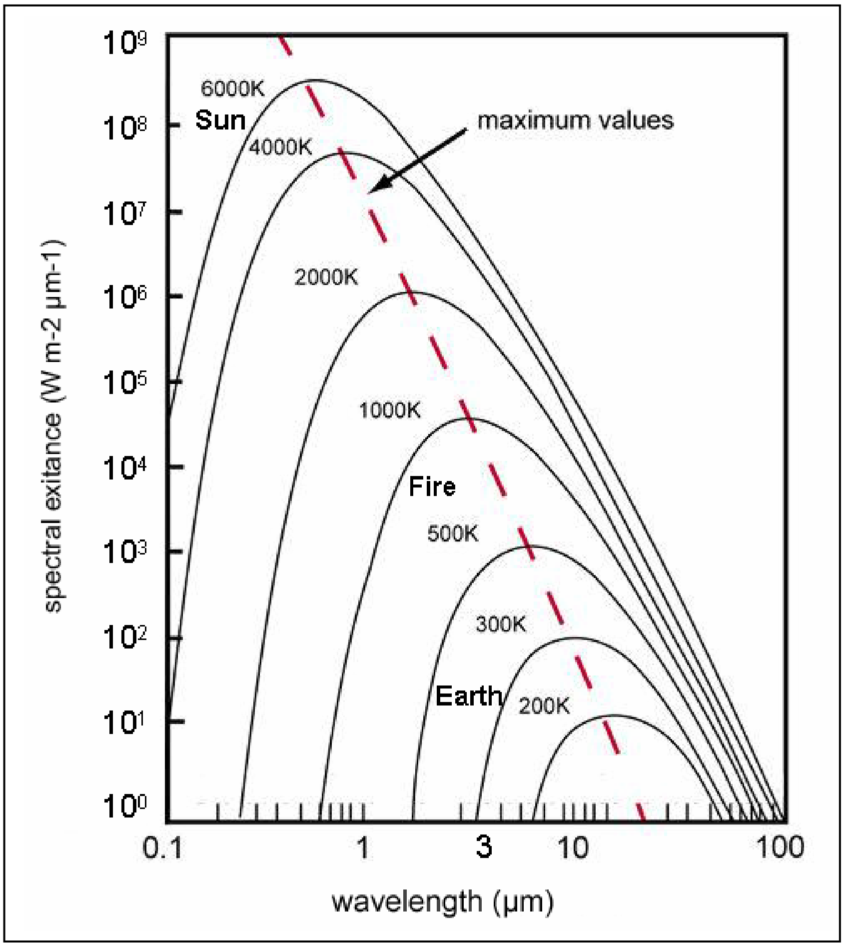

Figure 1.7. Emitted energy distribution for a blackbody at different temperatures.

One of the first sensors used for fire monitoring was the AVHRR of the NOAA satellite series (Flannigan and Vonder Haar, 1986). The AVHRR is a polar orbiting system with five channels in the visible and infrared domain; the spectral settings determine its capability to detect hot spots as fire. It has a spatial resolution of 1km and provides an image of the same area every 12 hours. Another sensor with similar characteristics is the ATSR (Along Track Scanning Radiometer) from which a global active fire product (World Fire Atlas) was derived for the period 1995-2006 (Arino et al., 2001). A more recent instrument with specific bands for fire detection is MODIS (Moderate Resolution Imaging Spectro-radiometer) on board the NASA Earth Observing System (EOS). Polar orbiting systems provide one or two images per day of the Earth surface. The temporal coverage of this type of sensors is not high enough for fire monitoring: all the fires occurring between the sensors overpasses are missed; in addition the presence of clouds, which can obscure fires, makes fire detection even more difficult, reducing the number of available observations. High temporal frequency is therefore essential if an effective assessment of fire activity has to be provided. Geostationary satellites, such as the Meteosat series, provide high temporal resolution imagery and have proved to be suitable for fire monitoring (Roberts et al., 2005).

Fire detection can be performed using automated algorithms and numerous methods have been developed (Flasse and Ceccato, 1996; Justice et al., 1993; Pozo et al., 1997; Li et al., 2000; Giglio, 2003). These algorithms can be classified into three categories:

- Single wavelength threshold,
- Multiple wavelength threshold,
- Contextual approach.

The first approach is based on the mid-infrared channel only. It uses the brightness temperature recorded in this spectral region because of its high sensitivity to fire. However, the MIR channel can be influenced by solar reflectance during daytime acquisition and highly reflective objects, like bare soil or clouds, can induce a strong spectral response which can lead to misclassification and commission errors. In addition, if problems of saturation occur they are more difficult to handle using this single-channel method.

The multiple wavelength method uses the brightness temperatures and the reflectance values recorded in the infrared and in the visible channels. Fixed thresholds are applied to the bands or to their differences (e.g. MIR and TIR). The use of more bands is useful to overcome some of the typical problems of fire detection. For example the bands in the visible region are used to mask clouds and the bright surfaces, whereas the mid- and thermal infrared channels are useful to reduce the number of false alarms: the difference between the two bands allows discriminating warm surfaces from the active fires since the MIR channel is usually more sensitive to high temperatures than the TIR and therefore a big difference between the two channels is indicative of a thermal anomaly. The combination of visible and infrared bands considerably improves fire detection.

The contextual approach is an additional improvement to fire detection algorithms; this method has been used for global and regional fire monitoring (Justice and Dowty, 1994; Justice and Malingreau, 1996; Eva and Flasse, 1996; Flasse and Ceccato, 1996; Dwyer et al., 1998). Fire is identified using the high contrast it shows when compared to the neighbouring non-fire pixels. The initial fire identification is made using fixed thresholds similar to those applied in the multiple wavelength method. This first part allows identification of potential fires. In the second step the potential fire pixels are compared to their immediate surroundings to test if their contrast is sufficiently high. In the positive case potential fires are confirmed, otherwise they are rejected. The surrounding pixels of a potential fire are identified using a window with varying size: the dimensions of the window depend on the sensor and the study area. Some statistical parameters (mean and standard deviation) are computed from this ‘contextual window’ and used for the comparison. This method shows more flexibility than the threshold-based approaches and therefore is suitable for different environmental conditions and ecosystems.

In order to improve fire algorithm performance, satellite data are usually previously masked to exclude some problematic features from the analysis. The most common masked-out classes are: water, reflective objects like clouds, bare soil and deserts.

1.2.2. Fire Radiative Energy

Besides active fires identification, fire activity can be further characterised considering its intensity that is the fire energy.

Energy is emitted in several forms: part of it is released as heat for convection, conduction and vaporization of water and gases, another important fraction of energy is released as radiation (Fire Radiative Energy, FRE).

FRE is the total amount of radiative energy released during the burning process; it is derived from the temporal integration of the instantaneous energy released which is termed Fire Radiative Power (FRP):

$$FRE = \int_t FRPdt \qquad [MJ] \qquad (4)$$

Fire Radiative Energy provides important information on the amount of biomass burned and has been proposed as an alternative method for burned biomass estimations in the context of fire emissions research (Wooster et al., 2003).

A relation between FRE and the rate of emissions released was first suggested by Kaufman et al. (1996) in the SCAR-C experiment, more insights were provided during the SCAR-B (Kaufman, 1998a, 1998b). The SCAR-C focused on fires in Northwest US (California) whereas the SCAR-B analysed fires in the Amazon forest and the *cerrado* of Brazil. The projects considered several aspects of fire activity, the most important of which are: smoke aerosols and trace gases emissions, burned areas and Fire Radiative Energy. Measurements of these parameters were carried out on the ground and using aircraft instruments and the fire spectral signature was recorded in the thermal and mid-infrared using the MODIS Airborne Simulator (MAS) which has proved to be particularly useful for fire observation (Kaufman et al., 1998c).

One of the most important findings of these experiments is the possibility of measuring the Fire Radiative Energy using spectral channels in the infrared domain. The MIR channel (centred at 3.9 μm) was recognized as particularly suitable because it is very sensitive to fire temperatures. In addition it was pointed out that Fire Radiative Energy and the rate of vegetation consumption are closely related. These conclusions gave ground to the use of satellite remote sensing for studies on vegetation fires and the related emissions.

There are several approaches which can be used for FRE estimation using satellite imagery. One of these is the Bi-Spectral method (Dozier, 1981) which uses fire signal recorded in the MIR and TIR bands. Fire is considered to have multi-thermal components with different temperatures and dimensions. FRP over all wavelengths is derived using the Stefan-Boltzman Law with the following equation:

$$FRP = \varepsilon_f \sigma \sum_{k=1}^{n} p_k T_k^{\ 4} \qquad [W] \qquad (5)$$

where

ε_f is the fire emissivity (grey body),

σ is the Stefan-Boltzman constant ($5.67 \cdot 10^{-8}$ J $s^{-1}m^{-2}K^{-4}$),

n is the number of thermal components of the fire,

p_k is the fractional area of the kth thermal component,

T is the kinetic temperature of the kth thermal component.

However, this method has some disadvantages since it requires information from two separate channels which can cover different areas. In addition fire temperature estimation, using the TIR channel, can be problematic because this spectral band is quite sensitive to the non-fire contribution of the background (Wooster et al, 2003).

This method is applicable to satellite sensors only if the instrument resolution is detailed enough to distinguish among different fire components. Usually an active fire detected from low spatial resolution imagery occupies only a fraction of a pixel.

In order to overcome these limitations other methods were developed to derive FRP from a single channel.

The first method to be introduced uses brightness temperature of the fire pixel in the MIR, which is particularly sensitive to the fire signal. This method has been developed by Kaufman (1996, 1998b, 1998c) to be applied on MODIS sensor.
Another approach has been proposed by Wooster et al. (2003, 2005) to derive FRP from low spatial resolution sensors, such as the geostationary systems. This approach has been implemented in small scale experiments and continental applications (Wooster, 2005; Roberts, 2005).

As with the previous method it requires information in the MIR channel only, but it uses the fire spectral radiance instead of the brightness temperature.

The approach applies the Planck Function [B(λ, T)] to show that the fire spectral radiance emitted in the MIR ($L_{f,MIR}$) can be approximated by:

$$L_{f,MIR} \approx \varepsilon_{f,MIR} a T^4 \quad (6)$$

where
$L_{f,MIR}$ is expressed in W m^{-2} sr^{-1} μm^{-1},
ε_f is the fire emissivity (grey body),
a is a constant empirically derived dependent on the wavelength and the temperature range chosen (W m^{-2} sr^{-1} μm^{-1} K^{-4}),
T is the kinetic temperature of the fire (K).

Equation 6 is valid for a range of temperatures which is typical of vegetation fires (500-1500K) and can also be written as:

$$L_{f,MIR} = a \varepsilon_{f,MIR} \sum_{k=1}^{n} p_k T_k^4 \quad (7)$$

where
a is a constant empirically derived dependent on the wavelength and the temperature range chosen (W $m^{-2} sr^{-1} \mu m^{-1} k^{-4}$),
$\varepsilon_{f,MIR}$ is the fire emissivity in the MIR (grey body),
n is the number of thermal components of the fire,
p_k is the fractional area of the kth thermal component,
T is the kinetic temperature of the kth thermal component.

Equation 7 is formally identical to equation 5 which expresses the energy emitted over all the wavelengths. If we equate these two relations, the FRP becomes independent of fire temperature and fire fractional area (T, p_k). Therefore the FRP over all wavelengths can be derived directly from the MIR radiance as is shown in the following expression:

$$FRP = \frac{\varepsilon_f \sigma}{a \varepsilon_{f,MIR}} L_{f,MIR} \quad (8)$$

Since the emissivity of fire is approximated to that of a grey body, its value is considered stable at all wavelengths ($\varepsilon_f = \varepsilon_{f,MIR}$). In order to derive the fire radiance, $L_{f,MIR}$, the contribution from the non-fire fraction in the fire pixel (that is the *background*) has to be removed from the signal on the active fire pixel. This is possible using the spectral radiance from the surrounding 'non-fire' pixels so that the fire spectral radiance, in the MIR, is expressed as:

$$L_{f,MIR} = (L_{p,MIR} - L_{bg,MIR}) \quad (9)$$

where

$L_{p,MIR}$ is the spectral radiance on the active fire pixel,

$L_{bg,MIR}$ is the spectral radiance of the background,

By taking into account these additional modifications and the pixel size (A_{samp}), the final expression of FRP as derived from the MIR radiance method becomes the following:

$$FRP = \frac{A_{samp}\sigma}{a}(L_{p,MIR} - L_{bg,MIR}) \quad (10)$$

where

A_{samp} is the pixel sampling area,

σ is the Stefan-Boltzman constant ($5.67 \cdot 10^{-8}$ J $s^{-1}m^{-2}K^{-4}$),

a is a constant empirically derived from the Planck Function (as in equation 6),

$L_{p,MIR}$ is the spectral radiance on the active fire pixel,

$L_{bg,MIR}$ is the spectral radiance of the background,

Equation 10 shows many advantages when compared to the formula used in the Bi-Spectral Method. Since it does not require information of sub-thermal fire components, it can be used for low resolution satellite sensors, where most fires have a sub-pixel size. Moreover, using only information from the MIR channel avoids channels misregistration and uncertainties in fire temperature estimations due to TIR channel. When compared to the single band method developed by Kaufman it has advantages because it can be applied to small and large fires, whereas the method developed for MODIS is more specific for small fires.

There are however some limitations in the MIR radiance approach. The method should be used only when fire temperature is greater than 600 K: for lower temperatures, or small fires, FRP can be underestimated. Underestimation is a common limitation which also affects the other methods described above. Although this is a disadvantage, small fires have a small contribution in terms of biomass burned and gaseous emissions which make this underestimation less crucial. Other factors which reduce the applicability of this method are the conditions that typically limit active fire detection from satellite imagery: clouds and the sun-glint effect. As such these disadvantages are also relevant to the other techniques used for FRP estimation.

Since the FRP value is an instantaneous value of radiant energy, it is necessary to integrate it over time if the whole amount of energy has to be derived (Fire Radiative Energy, FRE). This is possible considering the fire duration and the sampling frequency.

Once the FRE is determined, the biomass burned can be quantified using the empirical relation provided by Wooster (2005). This relation has been derived during a field experiment carried out in the African savannas. The vegetation burned is typical of savannas ecosystem (different types of grass) and was quantified measuring pre and post-fire biomass. FRP was measured using a field spectro-radiometer in different IR regions (range: 0.4-2.5 µm) and a MIR camera (3.6-5.0 µm). The burned biomass was compared with the FRE time series (derived using the MIR radiance approach). As a result the following linear relation could be derived:

$$\text{Biomass burned} = 0.368 \cdot \text{FRE} \qquad (11)$$

Since the spectral range available on the instruments is identical to that used by satellite sensors (e.g. MODIS, SEVIRI), the conclusions of the field analysis are also valid for satellite applications.

1.2.3. Burned areas

Although only active fire detection is performed in this work, the detection of burned areas is described in this paragraph to complete the review of available remote sensing approaches used for fire monitoring. Burned area mapping is also fundamental for the estimation of fire emissions because it provides the term *A (burned area surface)* used in the equation 3 (Section 1.1.3.).

Burned area left after fire occurrence shows a deposit of ash and charcoal formations. If the burned area is quite recent (usually few weeks) these features are usually detectable from satellite in the visible domain because the burned area appears darker than its surroundings (Pereira et al. 2003). Another effect of fire is the alteration of the vegetation status. This usually results in a more persistent signal which can be detected in the near-infrared (NIR) and the mid-infrared (MIR). The first shows a decrease in the reflectance values whereas the second registers an increase of the same parameter. Reflectance derived from these channels is used to produce burned area maps. The advantage of this approach, when compared to active fire detection, is the longer availability of the spectral signature. However, rainfall, vegetation regrowth and other environmental factors can affect the spectral signal and make it less contrasting with other land cover types (Justice et al., 1993; Barbosa et al., 1998; Eva and Lambin, 1998)

Several global burned area maps have been released in the last decade: they were derived from ATSR (Simon et al., 2004) and SPOT-Vegetation imagery (Grégoire et al., 2003; Tansey et al., 2004).

Chapter 2

2. Datasets

2.1. Case studies

Three fire events are selected as case studies for the satellite analysis. All of them occurred in Liguria (Italy). Two events happened almost concurrently from 14th to 19th February 2005. One site is located in Pegli (Genova) and the other one affected three communes (Stella, Celle Ligure, Varazze) in the province of Savona. The third case study is a fire from 2004 (6th to 8th September) which occurred in Sestri Levante. The information about the area burned is provided by the Italian Forest Service (Corpo Forestale dello Stato –Genova, Savona-). The exact location of the burned areas is shown in figure 2.1.

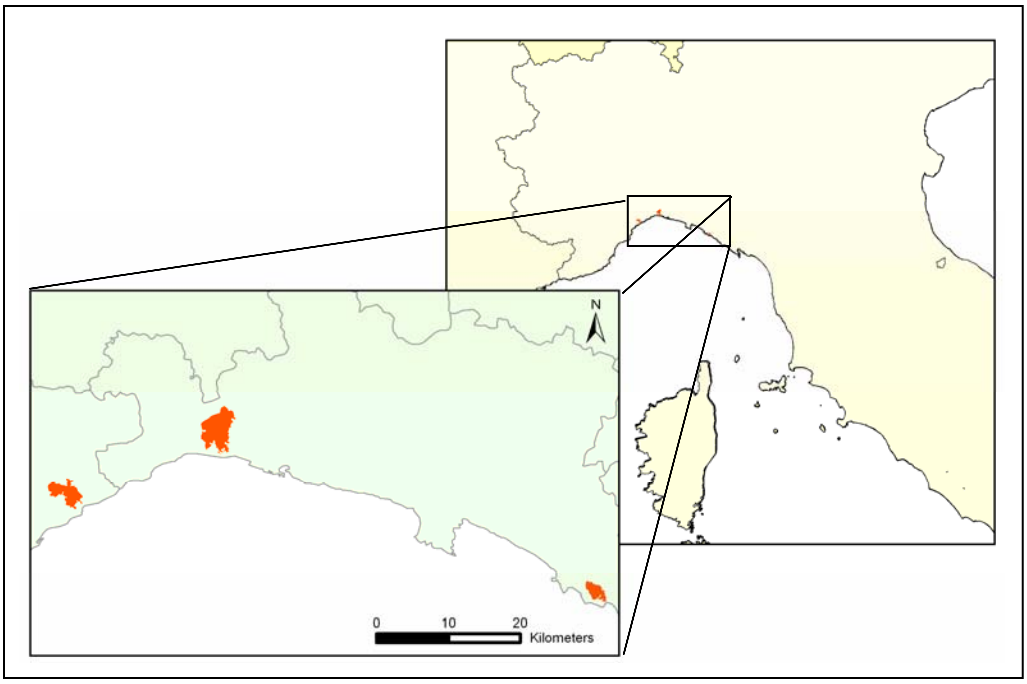

Figure 2.1. Case studies location.

The fire in Pegli was caused by arsonists. It affected an area of 1541 ha covered by Maritime Pine (*Pinus pinaster*), with an understorey mainly constituted by *Erica arborea* and *Arbutus unedo*. A few other species typical of the Mediterranean vegetation can be found in the area: *Rhamnus alaternus* and *Erica spp*. The fire was very intense and destructive because of the strong wind and the dry vegetation conditions. In addition, the dense understorey and the considerable number of pines affected by *Matsucoccus feytaudi* created ideal conditions for fire spreading. Pine trees with this type of pest usually show abundant quantity of resin along the bark which makes them very flammable. Maritime Pine is a very common conifer in Liguria covering an area of 29 000 ha (APAT, 2000), but the frequent fires and the parasites have significantly reduced its population.

The photos below show the effect of the fire which almost reached the city of Pegli .

Figure 2.2. Photo from helicopter of the area burned in Pegli.

Figure 2.3. Photo in the final phase of fire in Pegli.

Figure 2.4. Panoramic view of the Pegli site.

Figure 2.5. Snapped pine trees over the Pegli site.

Figure 2.6. A view of the slope in the Pegli site.

The fire occurred in the province of Savona during the same week of February 2005 shows similar conditions of burning (strong wind and dry vegetation) and vegetation type. Fire started because of human negligence affecting an area of 950 ha.

The fire that occurred in Sestri Levante started during the burning of agricultural waste which went out of control. The overall area burned is 505 ha. Vegetation, as in the other cases, is mainly composed of *Pinus pinaster* with an understorey of *Erica arborea* and *Arbutus unedo*. The fire was very intense because the pine forest was particularly flammable being affected by *Matsucoccus feytaudi.* In addition fire occurred during the summer season (early September) when weather conditions are still particularly favourable to fire spread (high temperatures and dry vegetation). The areas affected by the fire in Sestri L. are shown in the figures below.

Figure 2.7. Views of the burned area in Sestri Levante.

Figure 2.8. In some case the fire affected even the roots of the pine trees in Sestri Levante.

All the study sites are located in mountainous areas with steep slopes that typically lead to fast moving crown fires. A Digital Elevation Model is used to characterize the landscape topography over the burned areas. It is derived from the Shuttle Radar Topography Mission (SRTM). The original data has been reprojected into LAEA-ETSR89 and resampled to 100m resolution (Jarvis, 2006). The Digital Elevation Model (DEM) is shown in figure 2.9.

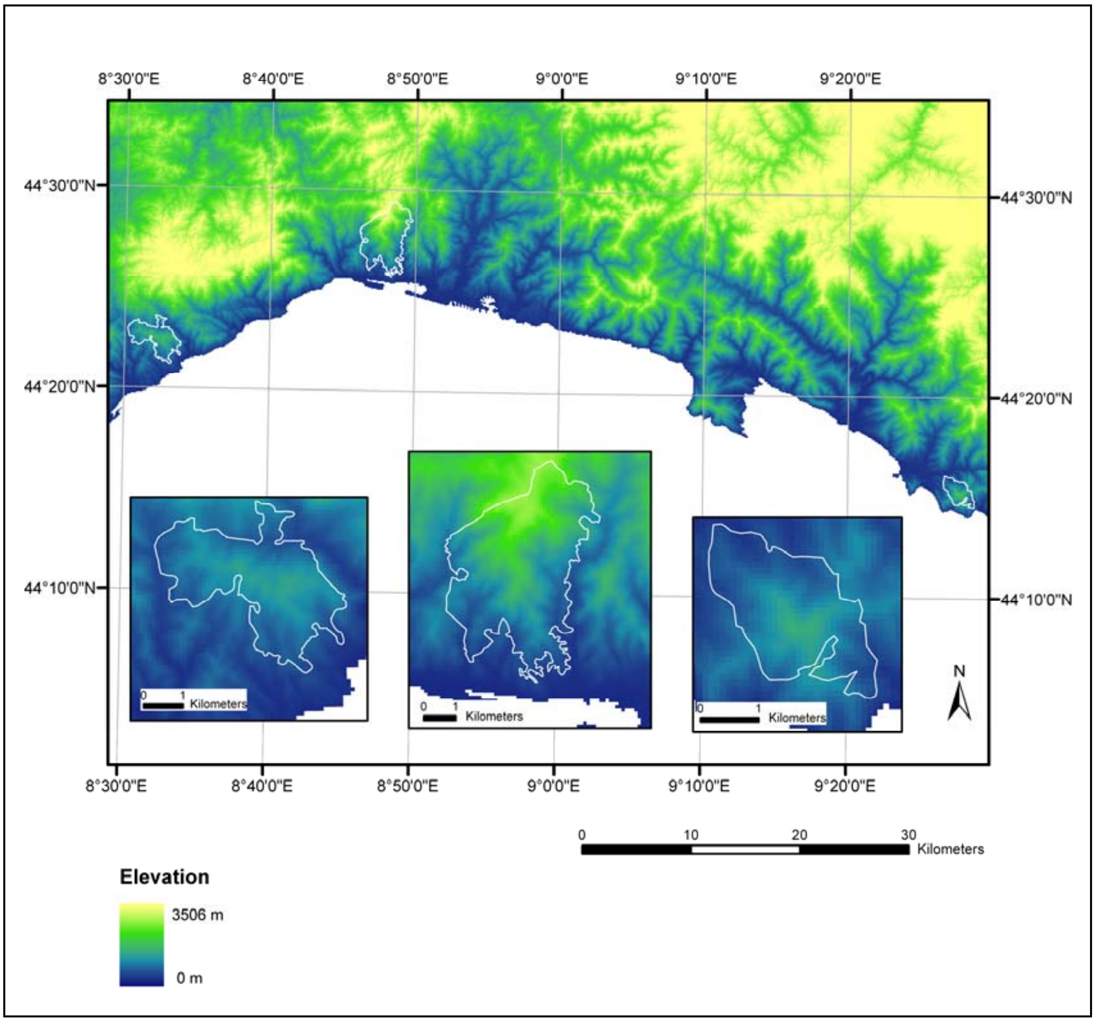

Figure 2.9. Digital Elevation Model over the three case studies.

The study areas have similar geology dominated by metamorphic rocks mainly constituted by serpentine, whereas in terms of soil type they show different classes as reported in the European Soil Database (http://eusoils.jrc.it/ESDB_Archive/ESDBv2/fr_thema.htm). The soil classes are based on the World Reference Base for Soil Resources (WRB) (FAO, 1998) and shown in figure 2.10.

The areas of Pegli and Savona are characterized by Dystric Leptosol (LPdy) which is typical of the Mediterranean region. This class is often present in hilly landscapes with steep slopes and shows a limited pedogenic development. Besides this soil type the area in Savona province shows the Eutric Cambisol type (CMeu) which is a young formation very common in the Mediterranean region.

The dominant soil class in Sestri Levante site is the Chromic Cambisol (CMcr) and Calcaric Regosol (RGca) which, as for the other areas, are not very much developed and typical of mountainous regions. Maritime Pine is well adapted to these soil types since it does not need rich or deep pedogenic formations.

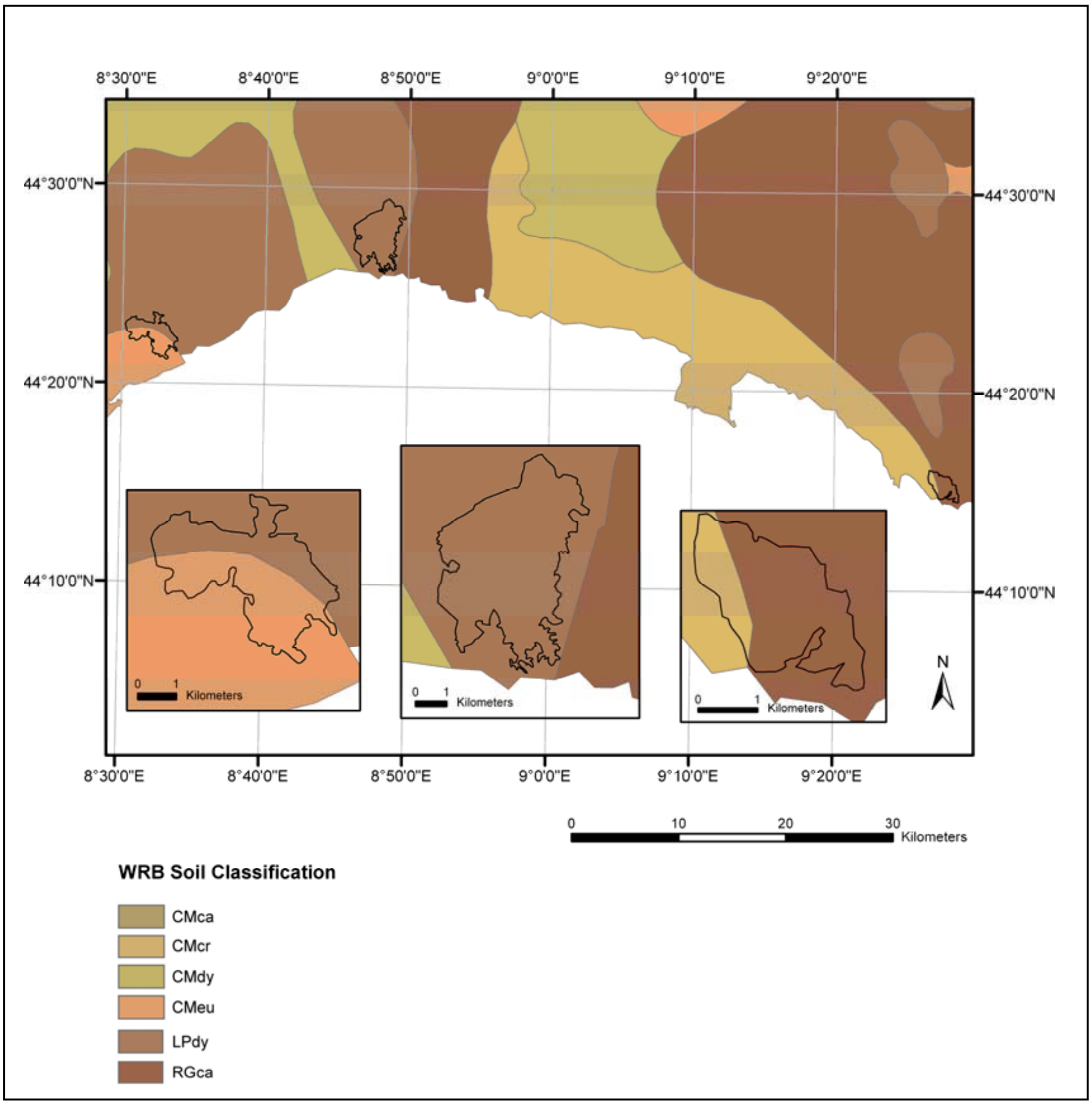

Figure 2.10. Soil type on the case studies.

The land cover type over the case studies is shown in figure 2.11., the classification used is the CORINE Land Cover 2000 ((http://terrestrial.eionet.europa.eu/CLC2000; European Commission, 2005) with a level-2 legend. The map derived from the Image 2000 is reprojected into LAEA-ETSR89 with a 100m spatial resolution. As shown by the map, the study sites are mainly covered by forest.

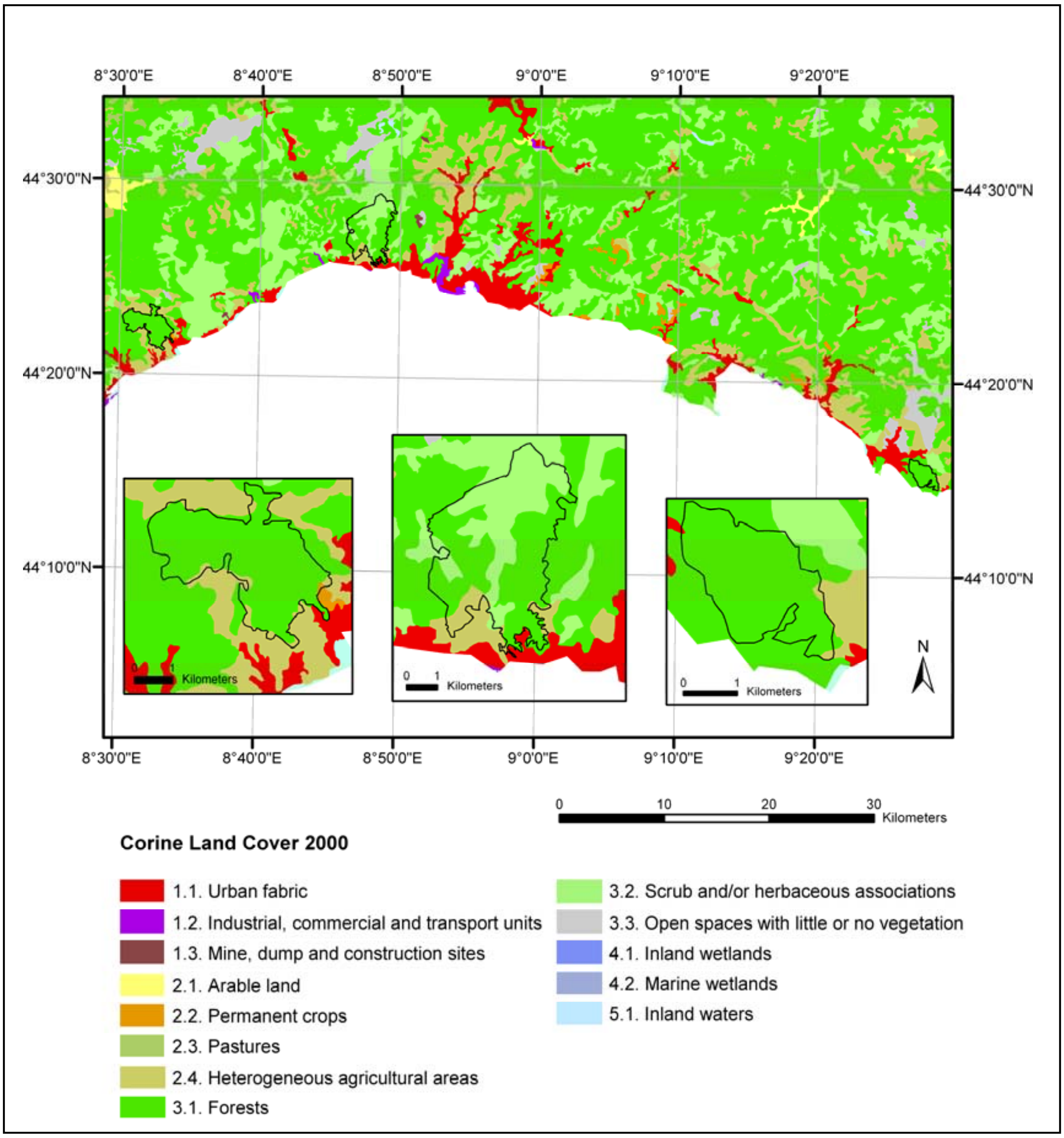

Figure 2.11. Corine Land Cover map for the case studies.

2.2. Field data

The fires that occurred in Pegli (2005) and Sestri Levante (2004) have been also studied in the field. Several campaigns were organized to collect data over the burned areas. Field work was carried out in August and September 2005. Burned areas were sampled using random circular plots in order to minimize the edge effect. The radius of the plot was defined to be 10m on a planar surface. The declination of the terrain varied between 9º and 38º therefore the radius was adjusted in order to have equivalent plots.

In order to establish the number of representative sampling plots for each study case, some preliminary surveys were carried out in the burned areas to collect information about the tree cover distribution and the degree of fire intensity (i.e. the level of damage on vegetation). With respect to these aspects both the areas presented little heterogeneity, however the sampled plots were distributed in order to be representative of the variability, in terms of fire intensity, within each site.

The Pegli site was sampled in six plots distributed over the burned area, whereas Sestri Levante, having a smaller burned area, was sampled in 4 different plots. The 'intensity of sampling', defined as the total area sampled divided by the total study area, is 1.85% and 3% for Pegli and Sestri Levante sites respectively.

For each sampled area the health status of vegetation and the level of damage were recorded. The main objective of the field measurements was the estimation of the above ground burned biomass. Vegetation volume, and consequently biomass weight, can be determined using information on the tree diameters at breast height (DBH) and tree heights (West, 2004). Although trees were heavily damaged, it was possible to measure these parameters (see figure 2.12.). The understorey layer was sampled as well by counting the number of shrubs on each plot and measuring the basal diameter and the plant major height (see figure 2.13.). The fractional coverage of the main species (*Arbutus unedo* and *Erica arborea*) was determined and the percentage of biomass burned was also estimated. All this information is used further in the analysis.

Figure 2.12. The sampled pine trees over the area burned in Pegli.

Figure 2.13. Measurement of the understorey basal diameter.

2.3. SEVIRI Sensor

The SEVIRI instrument (Spinning Enhanced Visible and Infra-Red Imager) was launched on board the Meteosat-8 satellite on 28 August 2002, becoming operational from January 2004 (Figure 2.14.). It is the first of a new generation of Meteosat satellites, known as Meteosat Second Generation (MSG). Originally these spacecraft series were developed for meteorological purpose only, however, with recent improvements, they are now also used to assess rapid changing phenomena like fires. Meteosat-8 satellite has a geostationary orbit. It is located over the equator where it crosses the Greenwich Meridian, at about 36 000 km altitude. Further details of the spacecraft are reported in table 2.1.

Source: Eumetsat

Figure 2.14. Meteosat-8 launched in August 2002.

Height above equator	35’786 km
Orbit radius	42’155 km
Arc length per degree	736 km
Orbital velocity	11’066 km/h 3.07 km/s

Table 2.1. MSG instrument details.

The area observed by Meteosat includes Europe, Africa, Middle East and the Atlantic Ocean (Figure 2.15.).

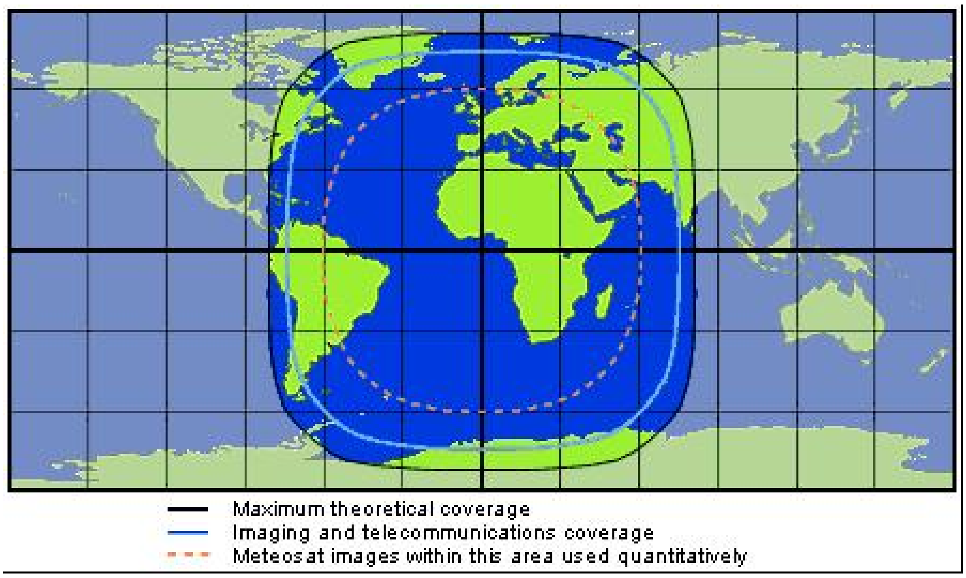

Source: Eumetsat

Figure 2.15. Observed area from Meteosat at 0 degree longitude.

Images are acquired using the combination of satellite spin and scan mirror rotation (stepping procedure). The instrument scans each line from east to west, and when the acquisition of one line is complete, the scanning mirror performs the stepping motion moving in the South-North direction. The nominal repeat cycle for a full disk scan takes 15 minutes, consisting of a period of 12 minutes for the actual scan and 3 minutes for retrace and on-board calibration. Images are acquired with a 10-bit radiometric resolution. The SEVIRI sensor has 12 spectral bands (Table 2.2.) acquiring information between 0.6 and 14 µm. Band 1 to 11 have a spatial sampling distance of 3 km at nadir and scan the full disk of the Earth; band 12 (also called High Resolution Visible, HRV) is a broadband visible channel with a higher spatial resolution of 1 km at nadir, it covers the full north-south extent of the disk as the other bands, but has a restricted east-west scan (Aminou et al., 1997). At mid latitudes the spatial resolution of a pixel decreases due to off-nadir imaging.

Channel number	Spectral Band (µm)	Spectral Range (µm)
1	VIS 0.6	0.56-0.71
2	VIS 0.8	0.74-0.88
3	NIR 1.6	1.50-1.78
4	IR 3.9	3.48-4.36
5	WV 6.2	5.35-7.15
6	WV 7.3	6.85-7.85
7	IR 8.7	8.30-9.10
8	IR 9.7	9.38-9.94
9	IR 10.8	9.80-11.80
10	IR 12.0	11.00-13.00
11	IR 13.4	12.40-14.40
12	HRV	Broadband 0.5-0.9

Table 2.2. Spectral bands characteristics of SEVIRI.

Particularly relevant for fire monitoring are MIR and TIR channels centred at 3.9 µm and 10.8 µm respectively. They are sensitive to high temperatures and therefore useful for active fire detection. Since the SEVIRI sensor has not been designed for active fire detection, saturation can be observed in the MIR channel when temperatures raise above 335 K. However, this is not very common because the low spatial resolution of the SEVIRI limits the size of the active fire to a small fraction of the pixel. Smoke can be identified by using the visible and near-infrared bands.

Raw data acquired by the SEVIRI instrument are preprocessed at EUMETSAT headquarters located in Darmstadt (Germany) and delivered as level 1.0 datasets. Images are also available at level 1.5 which is the format used in this study. These data are corrected for radiometric and geometric non-linearity and are accompanied by quality indicators, calibration and geo-location information. An example of the earth observed by MSG is showed in figure 2.16.

Source: Eumetsat

Figure 2.16. A color image from the Meteosat System.

2.4. Satellite Imagery

The images from level 1.5 are used for the analysis, they are available at Eumetsat archive (http://www.eumetsat.int/) and distributed in the geostationary projection, centred on 0º longitude. This projection is used in order to introduce the minimum distortion to the original data.

As described in the previous paragraph, the SEVIRI spatial resolution decreases moving off-nadir. Because of the geostationary orbit of the sensor the spatial resolution changes differently if moving along the parallel or the meridian axis and, as a consequence, the resulting pixels show a rectangular shape. At the latitude of the case studies (about 44 N) pixel size is around 3x5 km. In order to keep the original spectral information, the images are not reprojected into a regular grid, but they are analysed in the geostationary projection.

Images considered in the study include night-time and daytime acquisitions of the three case studies covering the whole fire duration. Satellite data are processed in order to i) identify the active fires with an implemented algorithm and ii) measure the radiant energy using the Fire Radiative Power approach.

Chapter 3

3. Methodology

The methodologies implemented in the present study are described in detail in this chapter. All the methods were applied on three selected case studies and each of them was dedicated to a specific objective of the work as it follows:

- the assessment of the active fires was carried out by implementing an algorithm for fire detection;
- the estimation of the amount of burned biomass was provided by applying the satellite approach which uses the Fire Radiative Energy (FRE);
- the preliminary validation of the FRE method was done by using the field data collected in the cases studies;
- the estimation of the gaseous emissions was fulfilled by using the information about burned biomass derived from the FRE application.

3.1. Fire Detection Algorithm

The identification of the active fires was carried out automatically with an algorithm for the fire detection which was implemented for the SEVIRI imagery. Satellite data were prepared for the analysis using some masking techniques so that the problematic features were excluded from the analysis. First of all a land/sea mask was applied in order to select only those pixels located on the land surface, this was done using the CORINE 2000. The Land Cover map was transformed into the geostationary projection of the SEVIRI imagery to make the two datasets overlap. Since the CORINE has a much higher spatial resolution (100m) than the SEVIRI images, the CORINE pixels were resampled within the SEVIRI pixel dimensions. The percentage of the SEVIRI pixel classified as "land" was then computed and only pixels with more than 50% of the "land class" were accepted for the analysis. This minimum fraction was chosen in order to include those pixels located along the coast line, which were potentially affected by the fire.

Cloud affected pixels were excluded from the processing by using a set of spectral thresholds which was defined according to the concepts suggested by Saunders and

Kriebel (1988). The brightness temperatures in the thermal and mid-infrared channels were used for this purpose. The appropriate thresholds were empirically defined combining the visual interpretation with the temporal series of the SEVIRI imagery. Images were also tested to avoid regions affected by specular reflection (sun-glint) and strong signal peaks, also termed 'hot-spot' effect (Myneni, 1994). Since the acquisition is made from a geostationary platform the sun and the satellite sensor are never in opposition at the considered latitude. However the sun angle and the sensor view angle can be similar when the sun is behind the sensor and this can result in the 'hot-spot' effect. This effect provokes an increase in the spectral signal which can result in false fire detection. Therefore the sun angles incident over the surface and the sensor view angles were computed and compared. If the differences of the zenith and azimuth angles between the sun and the sensor view were lower than 6 degrees, then the condition for 'hot spot' was fulfilled for these pixels. The 'hot-spot' effect is more pronounced in the red than in the near-infrared band because of the contrast between the sunlit and the shaded elements (Deering, 1989). Therefore a condition on the visible band (0.6 μm) was applied by using the Bidirectional Reflectance Factor (BRF) to identify and reject pixels affected by the 'hot spot' effect.

This band was also used to handle another issue which is the reflected component in the MIR domain. As shown in figure 3.1. at temperatures typical of the earth surface (300K), the MIR channel is a mixture of reflected and emitted signal; the two spectral components are equally present and it is very problematic to separate them (Doreen et al., 2004). Due to these spectral properties an object with high reflectance can have a strong response in the MIR channel without being a fire. Instead, the spectral signal of an active fire in the MIR (temperature around 900K) is mostly dependent on the emitted component since in this range of wavelengths the emittance is 10^3 times higher than the reflectance. The visible band was therefore used in the fire detection algorithm to reject pixels with high reflectance values.

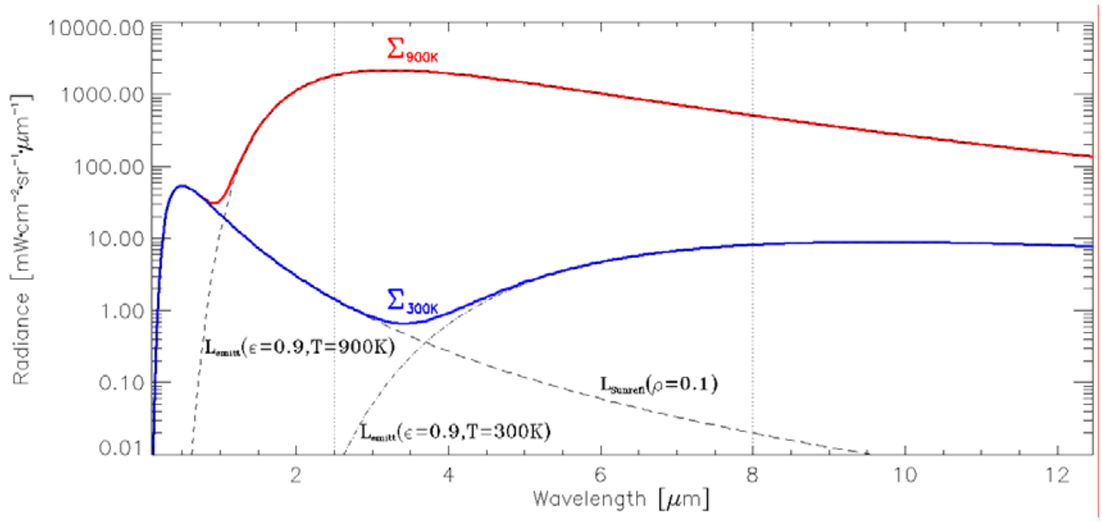

Elaboration by Peter Strobl.

Figure 3.1. The reflectance and emittance components of two objects at T= 300K (blue line) and 900K. The combination of these components provides the radiance spectrum shown in blue (T=300K) and red (900K).

The algorithm implemented for the fire detection is based on that used for the MODIS active fire product (Giglio et al., 2003a, 2003b). It uses a set of multispectral thresholds combined with a contextual approach as described in Section 1.2.1. They consist of a set of conditions applied to MIR and TIR brightness temperatures and also to the difference of brightness temperature in the two channels.

Since the satellite data include night and day time periods, they show a high variability in terms of solar illumination geometry which results in a variable spectral signal. In order to take these conditions into account the thresholds change according to the time of day and night. The selected values were specifically designed for the SEVIRI imagery and were empirically determined by analysing the datasets.

No atmospheric correction was applied to the MIR and TIR spectral bands because they coincide with two atmospheric windows where transmittance values are above 80% (Lillesand and Kiefer, 2000) and therefore they are not very much affected by the atmospheric effect. Also the visible band was not atmospherically corrected because the necessary information for this procedure (i.e. aerosol content, air humidity and temperature) is not available.

An additional condition was applied in the algorithm for fire detection to consider the pixels with high temperatures in the MIR and low temperatures in the thermal bands (band 9 and 10). This situation can occur because the mid and thermal infrared bands have different sensitivity to high temperatures as shown in figure 3.1. The radiance of an active fire (T=900K) in the MIR channel is about 10 times higher that recorded in the TIR band. Therefore when the background is ‘cold’ (at night or during the winter period), if a fire is under thin clouds or simply if the fire front occupies a very small fraction of the pixel it can happen that only the MIR band detects the active fire.

In these cases the thresholds for the fire detection applied on the MIR and on the difference between the MIR and the TIR brightness temperatures were different.

The pixels which fulfilled the set of conditions described above were classified as “potential active fire” and were further tested in the second part of the algorithm called the Contextual Fire Test. This additional criterion is particularly important when geostationary imagery is used. It is based on the spectral contrast which typically characterizes active fires and their background, therefore it is sensitive to fire even when variable environmental or illumination conditions are present (Flasse and Ceccato, 1996). Potential fire pixels (PF) and their surroundings were compared using the brightness temperatures in the MIR and TIR channels, and a set of statistical parameters derived from these values. A contextual window was used to identify the pixels around the PF. Pixels were considered suitable for the analysis if they were not a fire themselves or affected by clouds. The window had a variable size which was increased until a minimum amount of eligible pixels was reached.

The contextual test was carried out comparing the brightness temperature values over the PF to the statistics derived from the contextual window (mean and standard deviation of the brightness temperatures). If the differences between PF and the surroundings were above a fixed threshold, then the PF was confirmed, otherwise the PF was rejected. The processing chain followed in the fire detection algorithm is reported in figure 3.2. Details about the thresholds used for the fire detection are reported in chapter 4.

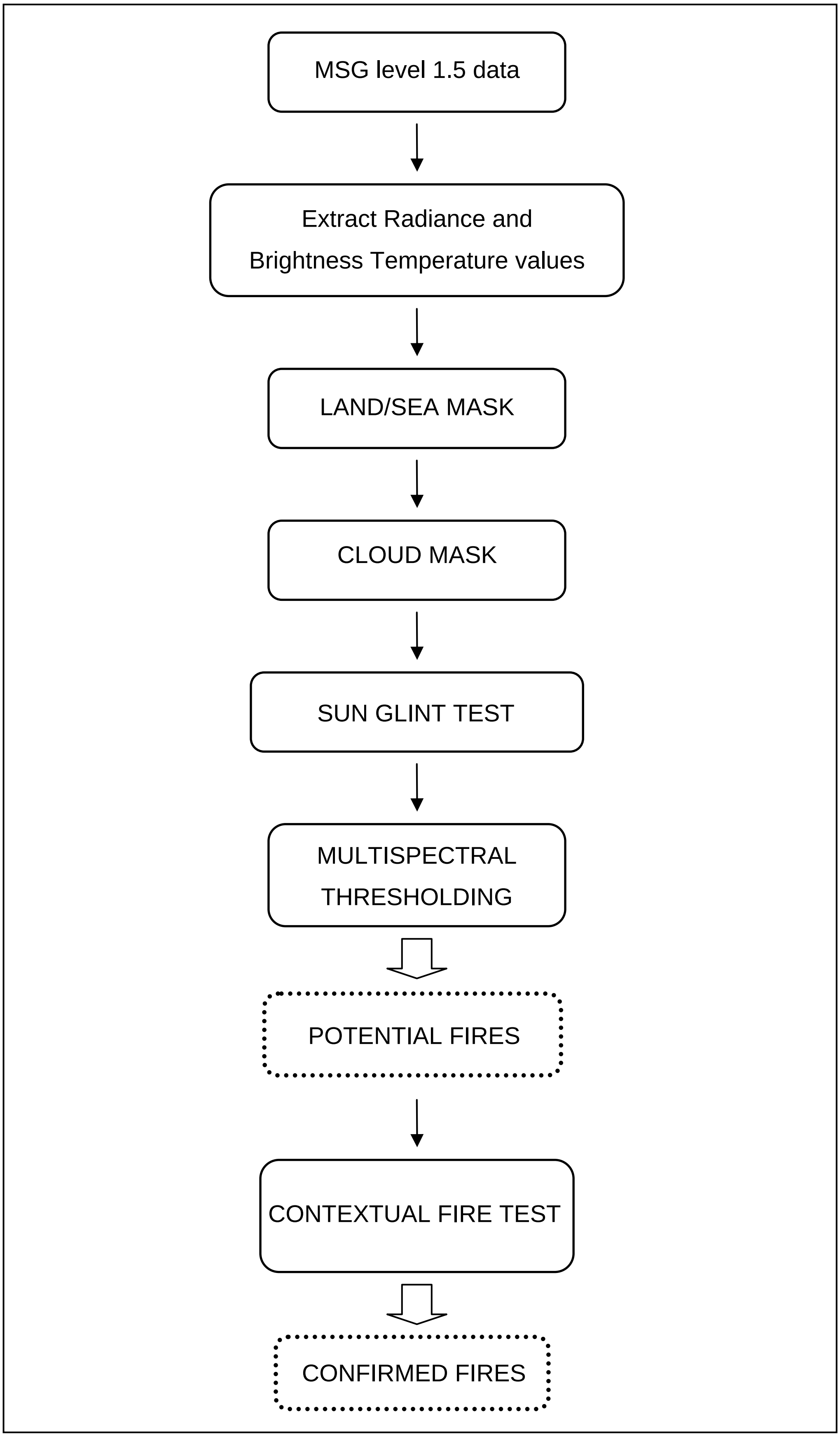

Figure 3.2. Fire Detection algorithm.

3.2. Retrieval of Fire Radiative Energy

Due to the high uncertainty attached to current burned biomass inventories, the quantification of burned biomass was performed using an alternative approach: the Fire Radiative Energy (FRE) (Kaufman et al., 1996; Wooster et al., 2005).

The radiant energy released was derived by using a satellite-based method which provides a measure of the instantaneous amount of energy: the Fire Radiative Power (FRP). The total amount of energy emitted during the combustion process was instead derived as the temporal integration of the FRP and this provided the FRE. This information was used to characterize the fire intensity and the amount of biomass burned.

The major advantage of this application is that no information on biomass density and burning efficiency is required. Drawbacks of traditional methods are that they use these two factors which are difficult to assess and are affected by high levels of uncertainties. Therefore improvements in burned biomass estimates are fundamental to assess the contribution of forest fires to greenhouse gas emissions.

In the present work the MIR radiance approach was used for the first time to derive the Fire Radiative Power in a Mediterranean ecosystem.

The MIR radiance technique was applied using the equation 10 presented in Section 1.2.2. The FRP was computed over the active fire pixels derived with the fire detection algorithm. Since a fire usually covers a small fraction of the SEVIRI pixel, the resulting spectral response is a mixed signal which also depends on the radiant contribution of the non-fire fraction. Therefore, when deriving the FRP, the spectral component of the part of pixel which is not affected by the fire has to be removed. Since the non-fire component cannot be directly measured, it was approximated to the radiance values of the pixels around the active fire, which were considered a valid reference for the non-fire fraction (Roberts et al., 2005). This group of pixels is termed *background.* In order to compute the FRP the radiance in the MIR band was derived over the fire pixel and the background contribution was subtracted from this value by using the mean radiance measured over the background.

Background characterization can be problematic especially in the Mediterranean region. Differently from the savannas ecosystem, where the methodology has been developed, the Mediterranean region shows a higher spatial heterogeneity and landscape patterns are more fragmented. In addition to the environmental conditions the image pixel size is bigger than in the tropical area, and this combination increases the variability of surface features included in one pixel. This results in a mixed spectral signal which affects the background characterization and the fire signal itself.

In order to tackle all these different conditions two main changes were introduced to the MIR radiance method. They were applied to the background characterization and are the following points:

- the background window dimension,
- the conditions for the selection of the pixels used as background.

The background window has fixed dimension (5x5) to identify the pixels around the active fire. The dimension guarantees to use only those pixels close to the fire: this increases the probability that they have spectral characteristics similar to that of the fire pixel. The immediate surrounding pixels (3x3) were excluded because their signal could be affected by that of the fire due to the partial overlap of the instrument Point Spread Functions (PSF). With this condition the resulting window looks like a ring surrounding the fire pixel. Pixels included in the ring were considered eligible for background characterization if they were not a fire or a cloud and had a land-cover type similar to that of the fire pixel. This last constraint was adopted to select pixels with spectral characteristics representative of the fire background. The land-cover type was defined using the CORINE 2000 Land Cover map. As for the fire algorithm the land cover map was converted in the geostationary projection of the SEVIRI imagery and the pixels were resampled so that the datasets could overlap.

The FRP was derived for each fire pixel using the formula 8, and then the pixels were clustered by using some spatial criteria (i.e. pixel adjacency) in order to identify the pixels which belong to the same fire. In this way the FRP was cumulated over a single fire. The processing chain for the FRP computation is outlined in figure 3.3.

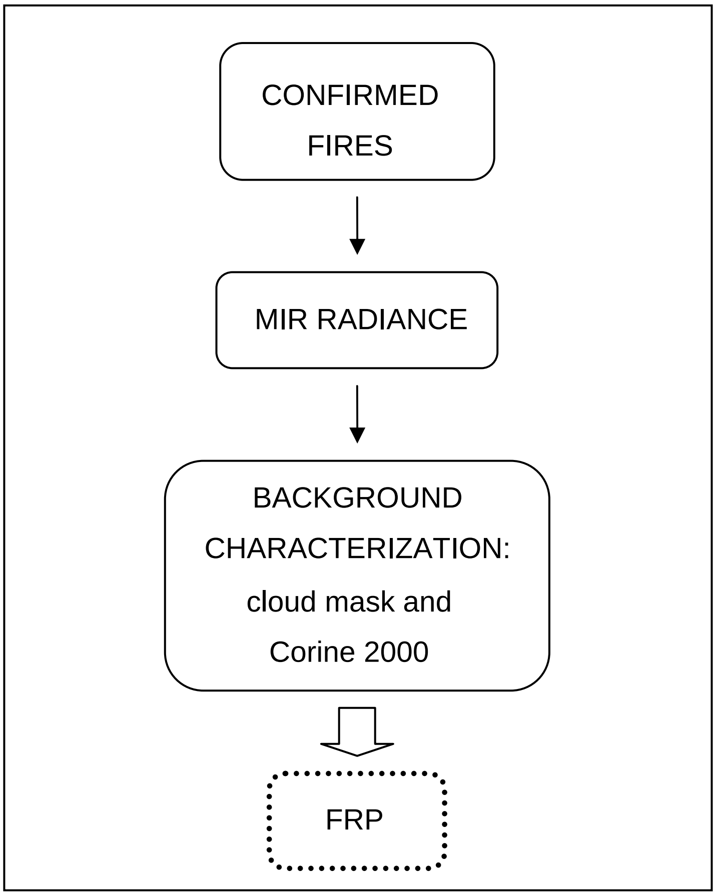

Figure 3.3. Processing steps for the FRP estimation.

Since the FRP values are an instantaneous measure of the fire energy, the total amount of energy emitted (FRE) was computed by integrating the FRP over time which is the whole fire duration (see equation 4). The integration was made by considering the instantaneous FRP as constant over the 15 minutes of acquisition.

3.3. Burned biomass estimation

The amount of burned biomass was derived from the FRE using the equation 11. Although this empirical relation was derived from field data of a tropical area, it is considered suitable for this study since it is demonstrated that the relation is independent of the vegetation type (Wooster et al., 2005; Lobert and Warnatz, 1993; Whelan, 1995; Trollope et al., 1996). The estimates of burned biomass derived with the satellite application were used for the quantification of the fire emissions. They were also compared to other estimates derived from data collected in several field campaigns which were carried out in three study areas, in Italy.

Usually the estimates of vegetation biomass derived from the field measures show a level of accuracy around 15% (Bagnaresi et al., 1987), therefore in this study this information was used as a reference to evaluate the level of accuracy of the burned biomass estimates derived from the FRE.

Tree biomass is usually determined using information on tree diameters at breast height (DBH) and tree heights. All the tree diameters within one plot were measured, and also most of the tree heights. The tree heights not directly measured in the field are calculated using the relations between the DBH and the heights derived from the available datasets. These parameters were necessary to define biomass volume and, once this was derived, the amount of biomass as dry weight was calculated using the wood density of the tree species (West, 2004). Vegetation volume was calculated using the regression functions derived by ISAFA (Istituto Sperimentale per l'Assestamento Forestale e per l'Alpicoltura).

Above ground burned biomass was defined as the difference between the pre-fire biomass load and the post-fire unburned biomass.

Pre-fire vegetation was defined as dendrometric biomass, this means that the complete tree volume, except the roots, was considered. The appropriate function for computing this was derived from a table by Meschini (ISAFA, 1970) which provides dendrometric volumes per different diameter classes, height information is not included. The table was built up using 100 trees sampled in San Rossore (Tuscany) belonging to a general fertility class.

The estimation of post-fire biomass was done considering the stem volume since most of the trees on the burned areas were snapped or with only part of the canopy. The relation used for the volume computation was derived from a table by Benassi (ISAFA, 1970). The table provides stem volumes using trees diameters and heights. The dataset was derived from 336 trees sampled in Tuscany, the sample data refer to a unique fertility class. The additional use of tree height, in the regression function, was particularly important to better estimate post-fire biomass. As a matter of fact, many trees were damaged by fire and therefore showed a reduced height which needs to be taken into account.

The biomass burned of the understorey layer was quantified using information collected in the field and data about the fuel load of the plant species derived from literature (Viegas, 1989).

Information about the field measurements and the results of the analysis are reported in Chapter 4.

3.4. Emissions estimation

The information about the burned biomass derived from the FRE was finally used to estimate the fire emissions relative to the case studies considered in the analysis. The main greenhouse gases and the particulate matter were taken into account since these components are the more relevant in terms of the amount of emissions and the atmospheric impacts. The emissions were estimated using the equation 2 proposed by Seiler and Crutzen (1980). More details about this formula are provided in chapter 1 (Section 1.1.3.).

The emission factors used are those found in the literature (see Andreae and Merlet, 2001) and are reported in table 3.1. Since there are not specific emission factors for the Mediterranean vegetation type the values from the "Extratropical Forest Class" were considered. The level of uncertainty attached to the values is also indicated (only for a few species this is not available).

Species	Extratropical Forest
CO_2	1569 ± 131
CO	107 ± 37
CH_4	4.7 ± 1.9
NMHC	5.7 ± 4.6
CH_3Cl	0.050 ± 0.032
PAH	(0.025)[a]
NO	3.0 ± 1.4
N_2O	0.26 ± 0.07
NH_3	1.4 ± 0.8
HCN	(0.15)[b]
$PM_{2.5}$	13.0 ± 7.0
BC	0.56 ± 0.19

Source: Andreae and Merlet, 2001

[a] Estimate is based on laboratory studies;

[b] Value is best guess.

Table 3.1. Emission factors of the main chemical species released. Values are gram of species per kilogram of dry matter burned.

4 Chapter

4. Results

4.1. Active fire maps

In this section the details of the algorithm for active fire detection are presented and the resulting active fire maps are shown and discussed.

An image of the active fires in Pegli and Savona is shown in the figure 4.1., the smoke plumes are enhanced using a false colour composite of the infrared and visible bands. The shape of the smoke plumes indicates the direction of the wind which blows from north to south.

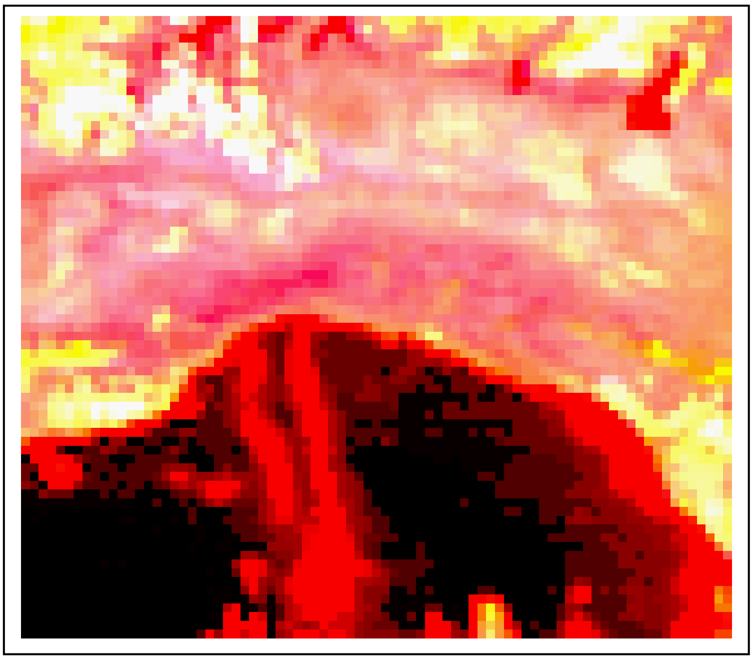

Figure 4.1. False Color Composite of SEVIRI image (15th February 2005, 13.12 UTC time. R: VIS 0.6 µm; G: VIS 0.8 µm; B: NIR 1.6 µm)

Another image of the fires in Pegli and Savona is shown below (figure 4.2.), the fires are observed in MIR channel. The corresponding transects across the fires are reported in figure 4.3. and 4.4. which show the spectral signal in the MIR and TIR bands considering the radiance and the brightness temperature values respectively.

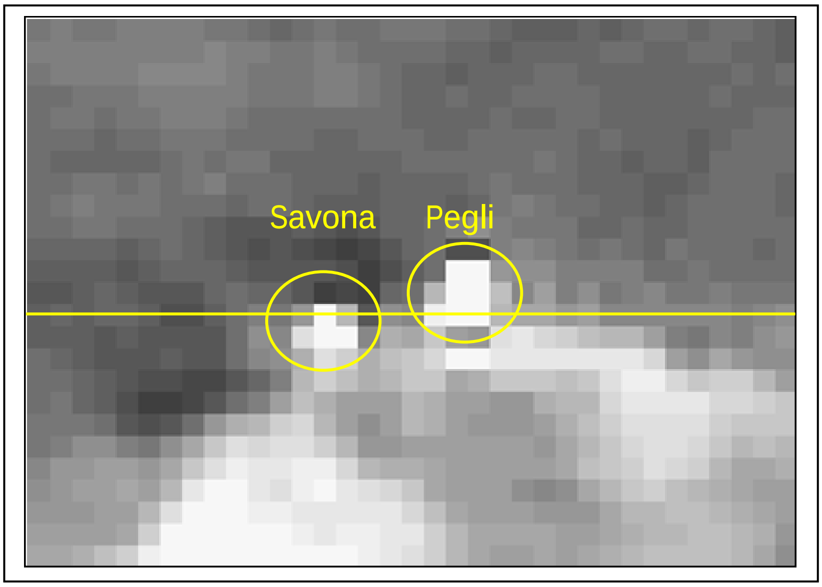

Figure 4.2. Fires on a SEVIRI image (date: 15th February 2005, 23.27 UTC; MIR: 3.9 µm).

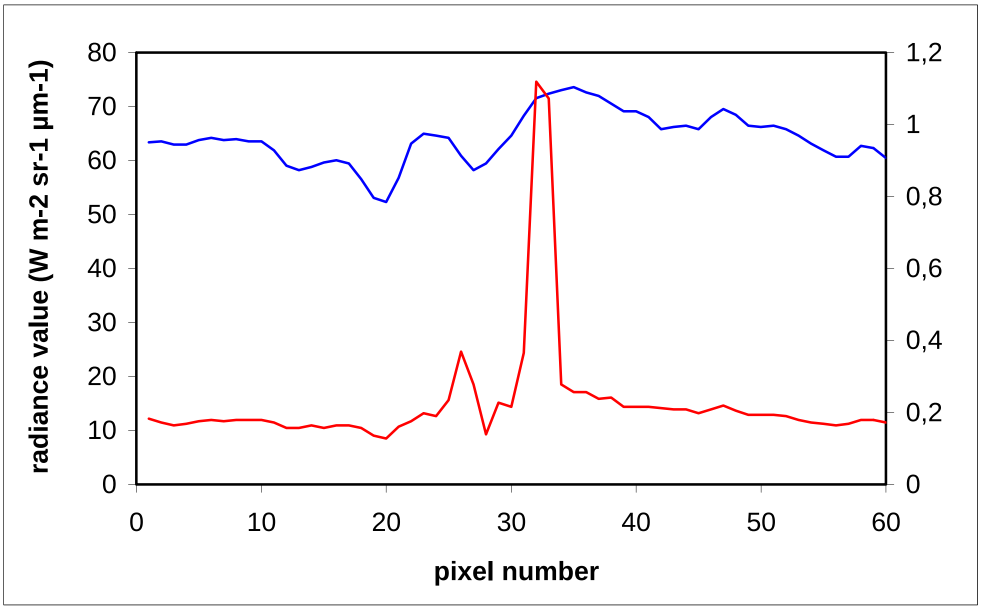

Figure 4.3. Spectral profiles in the MIR and the TIR moving west-east over the active fires.

The radiance values in the MIR and TIR bands show a peak over the active fires, the absolute values are different since the wavelengths are located in well separated spectral domains as described by the Planck's Law. When the radiance is converted into brightness temperature values, the two bands are more easily comparable as shown in figure 4.4. Since the MIR has a stronger sensitivity to high temperatures it registers a more evident response than the TIR. Because of their spectral properties these bands are used for the identification of the active fires.

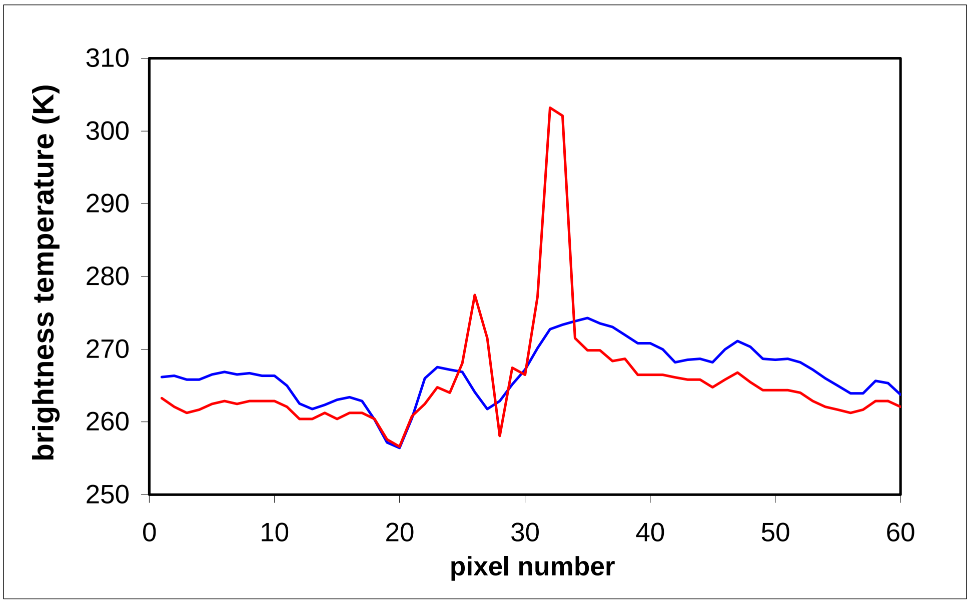

Figure 4.4. Profile of brightness temperatures in the MIR and TIR channels, moving west-east over the active fires.

In order to carry out the fire detection the satellite images are prepared in the following way:

- a land/sea mask is applied using the CORINE 2000 to exclude pixels with more than 50% of the class 'sea';
- a cloud mask is derived by visual interpretation and by using the time series of day and night acquisitions.

The cloud mask is derived by using the brightness temperatures in the band 4 (3.9 μm), 9 (10.8 μm) and 10 (12 μm). They correspond to the MIR and TIR spectral domains and the thresholds are reported in table 4.1. Different values are used for day and night images, since the illumination and the surface temperature change during the 24h period and this affects the final spectral signal.

Time of day (hhmm)	Band 4 (K)	Band 9 (K)	Band 10 (K)
Day time (6.01- 19.59)	262	259	259
Night time (20.00 - 6.00)	258	259	259

Table 4.1. Thresholds applied for cloud masking.

The datasets are also processed in order to avoid abnormal values due to saturation: if a pixel in the MIR band shows a brightness temperature of 0K, the value is replaced with the maximum temperature recorded over the whole image. Usually those anomalous values are found in the along-scan direction next to an intense fire with temperatures close to the saturation point, 335K. As shown in figure 4.5. the pixels around the active fire have a lower spectral signal which is particularly evident over the pixel at 0K. This anomaly has been already observed in a SEVIRI image of Southern Africa and the effect is named ‘pixel bleeding’ (Wooster and Roberts, 2004)

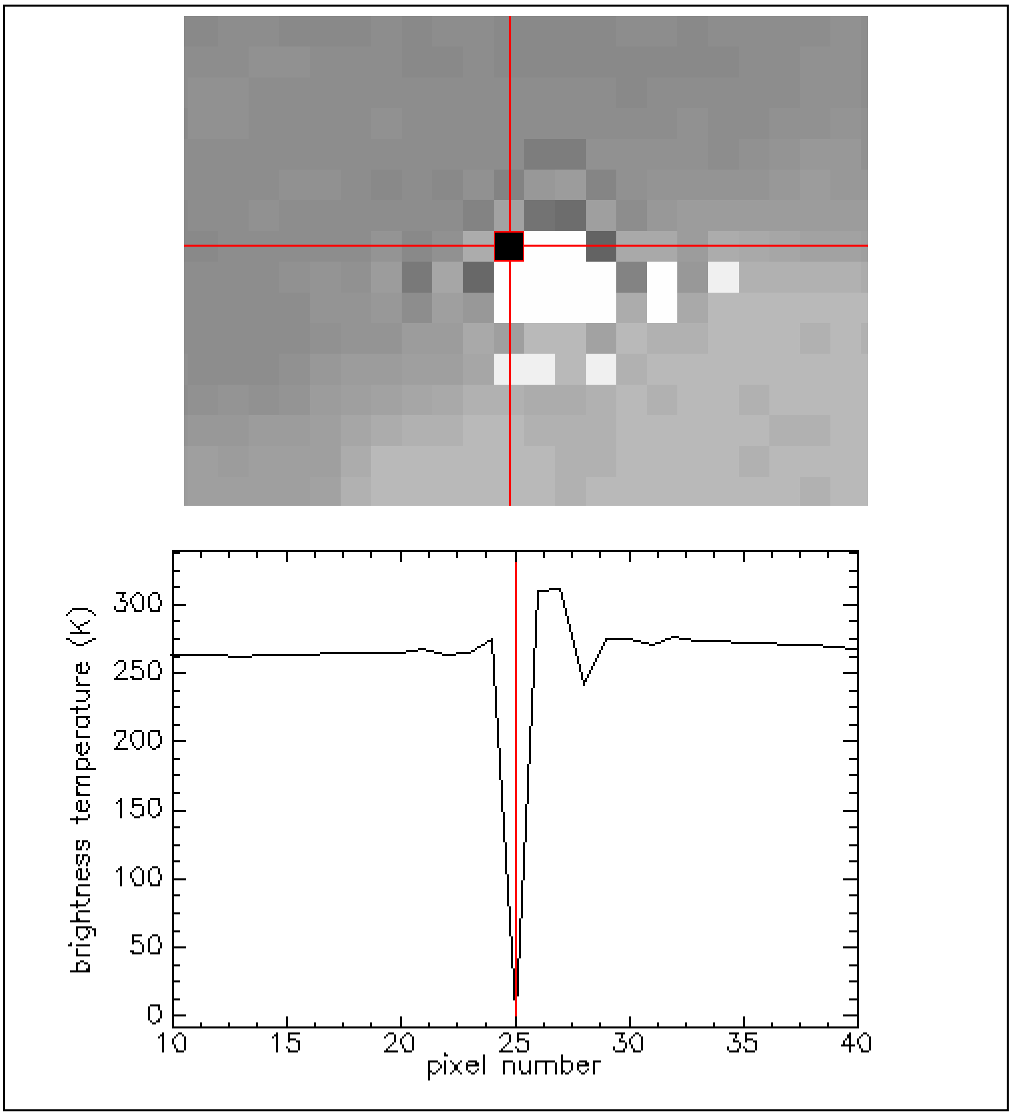

Figure 4.5. The saturation effect over an active fire in the MIR band (Pegli, 14 February 23.42 UTC).

Cloud free pixels are processed in the fire detection algorithm by using the brightness temperatures in the MIR and TIR channels and their difference as shown in table 4.2.

Time of day (hhmm)	Threshold (K)
0800-1400	T4 > 287, T9 > 284, ΔT > 5
1401-1959	T4 > 288, T9 > 281, ΔT > 7.2
2001-0759	T4 > 286, T9 > 280, ΔT > 8

Table 4.2. Set of thresholds applied to SEVIRI images during the 24-hour acquisition. T4 is the brightness temperature at 3.9µm. T9 is the brightness temperature at 10.8µm and ΔT is the difference of brightness temperatures: T4 - T9.

The conditions are common for all the case studies and are adapted to the variable periods considered: February and September. They are empirically defined by analysing the SEVIRI time series and change according to the time of image acquisition since the ambient background temperature is different on daytime and night-time images.

The brightness temperatures in the MIR and TIR are also used to apply an additional condition which tests the pixels in case of a 'cold' background (normally at night, during winter or if thin clouds are present). This test is important to take into account the different spectral responses of the two bands as shown in figure 4.4. If the pixel temperature in the thermal infrared channels (9 and 10) is below 280K and in the MIR is above 283K (at night-time) or 287K (daytime) then it is possible that a thermal anomaly is present but it is not clearly indicated by the thermal infrared. Therefore the pixels which satisfy these conditions are tested using thresholds different from those presented in table 4.2. The test criteria request that the pixel has a brightness temperature higher than 287K in the MIR (regardless it is day or nighttime) and the difference of brightness temperatures between channel 4 and 9 is higher than 10K. Examples of pixels with this type of behavior are found in the imagery from mid-February 2005 at nighttime.

In addition to the infrared channels the visible band 1 (0.6 µm) is also used to implement the fire detection algorithm. A condition on the Bi-directional Reflectance Factor (BRF) is applied to avoid pixels with high reflectance values. Moreover it is useful to handle pixels affected by 'hot spot' effect. Those pixels are observed on images acquired around 12.30 pm when the view zenith and azimuth angles are similar to those of the sun with differences lower than 6 degrees.

The condition on BRF reduces the number of false alarms and limits the effect of backscattering since pixels with high BRF are not considered as ‘potential fire’. For the cases of Pegli and Savona the same condition is applied: the pixels are considered as potential fires if the BRF values are lower than 0.24. For the site in Sestri Levante the condition is different: values are accepted if lower than 0.20. This threshold is applied because the criteria used for MIR and TIR brightness temperatures (table 4.2.) are less strict for the case of Sestri Levante since the images from September can have higher temperatures compared to those of the other sites from February. Therefore, in order to limit the number of false alarms the condition on reflectance is more rigid for Sestri Levante.

Once the “potential fire” pixels (PF) are identified, the contextual test is performed considering the PF pixels only. A set of statistical parameters is derived from the PF and the surroundings pixels (background) in the MIR and TIR bands. The pixels of the background are identified using a contextual window of variable size. It is enlarged until a minimum amount of eligible pixels (20%) or the maximum dimension of 9x9 pixels is reached. This dimension is fixed by taking into account the SEVIRI pixel size in order not to include pixels located too far from the potential fire.

The statistical parameters used for the contextual test are the mean and the standard deviation derived from each PF and the correspondent background. A potential fire pixel is confirmed if both the conditions reported in table 4.3 are satisfied.

Contextual Test conditions
PF4-PF9 > max (bg4-9 + 2.0 * sd4-9, 3.0)
PF4 > (bg4 + sd4 + 2.0)

Table 4.3. The conditions applied in the contextual test. PF4 is the brightness temperature in band 4 of the potential fire pixel; PF9 is the brightness temperature in band 9 of the potential fire pixel; bg4-9 is the mean value of (T4- T9) in the background; sd4-9 is the standard deviation of (T4- T9) in the background; bg4 is the mean value of T4 in the background; sd4 is the standard deviation of T4 in the background.

The active fire maps derived over the case studies of Pegli and Savona are presented in figure 4.6. The maps report the number of fire detections over the same pixel during 5 days (14-18 February). Map a) represents the active fires derived by applying the criteria for the fire detection without the condition on the BRF. Whereas map b) shows the improved result obtained when the threshold on BRF is applied.

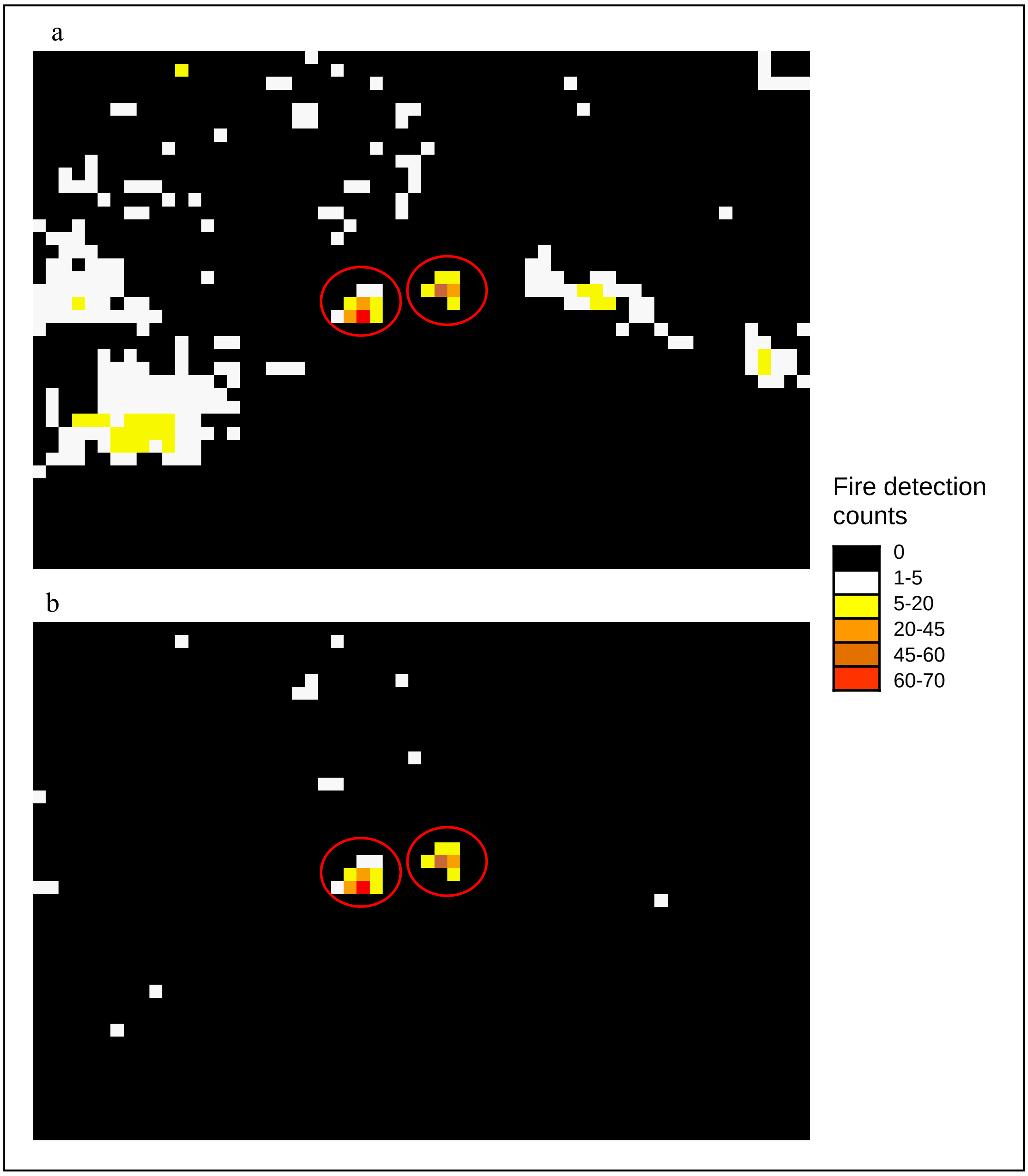

Figure 4.6. Active fire detection using the algorithm (a) without the condition on BRF and (b) with a constraint on BRF (0.6µm).

Most of the false alarms are detected during day time and depend on the solar reflective component in the MIR band. When the condition on BRF is applied the the number of false alarms is reduced by 93%.

4.2. Fire Radiative Power

As described in Section 3.2. the Fire Radiative Power is derived using the radiance measured over the fire pixels and that derived from the background (in the ring window). The percentage of eligible pixels used for the background characterization, over the total amount of pixels in the ring, shows that around 90% of the fire pixels has a background with more than 50% of eligible pixels, and only 1% of the fire pixels shows a background with less than 20% of eligible pixels. This indicates that the fire background is characterized in a representative way although the window used for this has a limited size.

In figures below the time series of the FRP are reported for all the case studies. In terms of radiant energy the fires in Pegli and Sestri Levante reach the same peak: about 2800 MW; whereas the fire in Savona shows an instantaneous value higher than 5000 MW which indicates a more intense fire activity. This is however better understood when the total amount of radiant energy is considered (FRE).

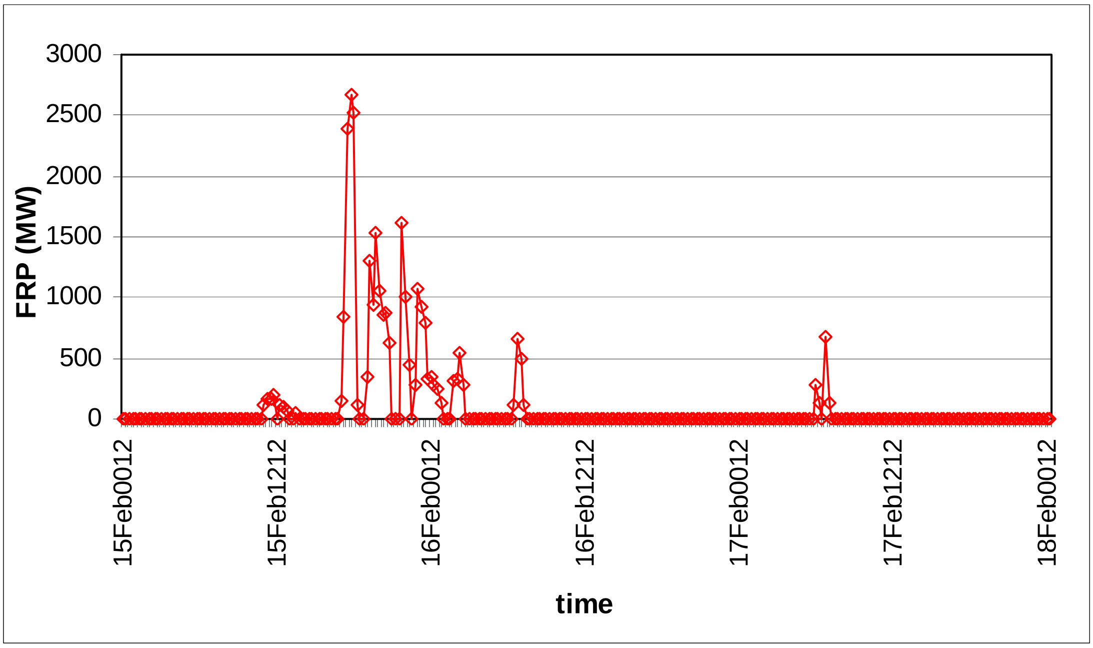

Figure 4.7. The FRP time serie in the Pegli site.

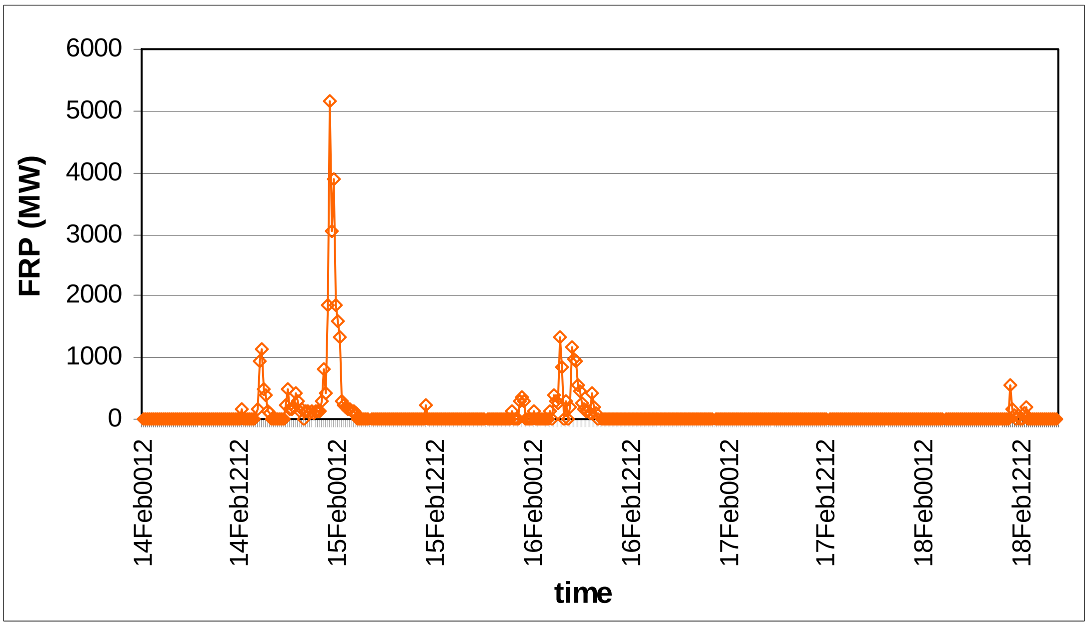

Figure 4.8. The FRP time serie in the Savona site.

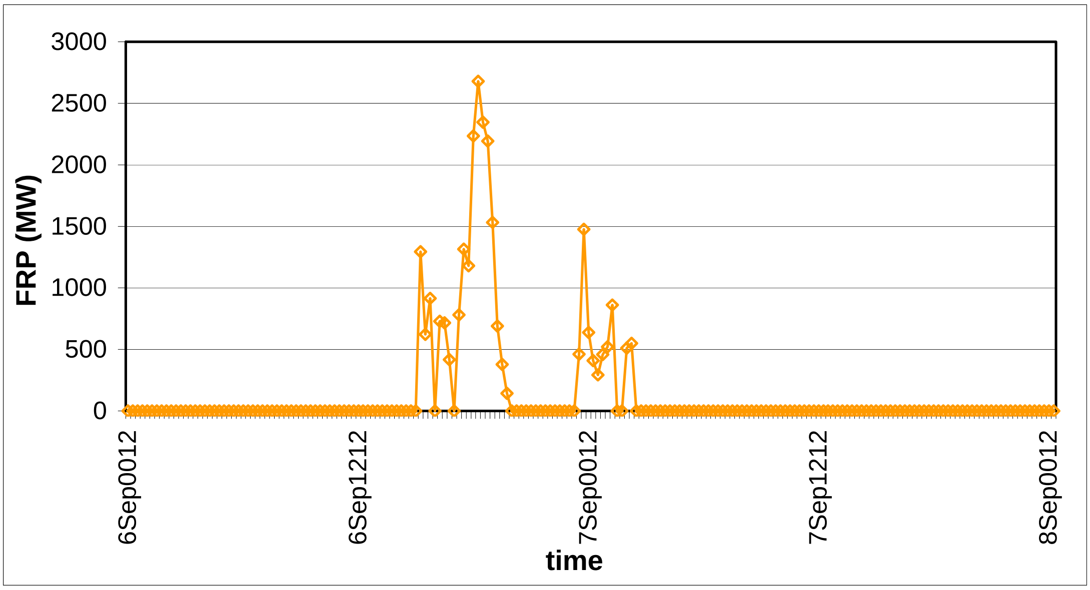

Figure 4.9. The FRP time serie in the site of Sestri Levante.

The analysis of the FRP shows that the fire in Pegli lasts from 15th of February until 17th, whereas in the site of Savona the fire activity has a longer duration, from 14th to 18th of February. The fire in Sestri Levante lasts from 6th to 8th of September. These durations are also confirmed in the reports by the Fire Brigades. Fire activity is discontinuous with peaks of high intensity and periods of decrease. Fire activity shows several phases also depending on the changing weather conditions (wind drop or increase) and the actions carried out for the fire suppression as documented in the bulletins from the Forest Service (CFS) and the Fire Brigade. However the gaps in the fire activity might have also other causes like the presence of clouds. Therefore the cloud cover over each fire is computed and the results are shown in figures 4.10 and 4.11. The cloud cover is derived from the cloud mask used in the fire detection algorithm. It is expressed as the percentage of fire pixels, of the same fire, classified as ‘cloud’.

The comparison of the FRP time series with the cloud cover shows that there is often a correspondence between the decrease or the absence of the FRP values and the presence of clouds, especially when the percentage of cloud cover is above 50%. In these cases the FRP can be underestimated since the presence of clouds limits the detection of the fires and as a consequence the FRP is not computed. The missing FRP values can be derived by interpolation from the time series to compensate for this effect. Cloud cover is shown for the case studies of Pegli and Savona. Although in Sestri Levante no clouds are detected, there are some gaps in the FRP time series because some images are missing from the Eumetsat archive. The missing acquisitions are on the 6th September at 1.27am and 10 images on 7th September between 1.42am and 4.12am are not available.

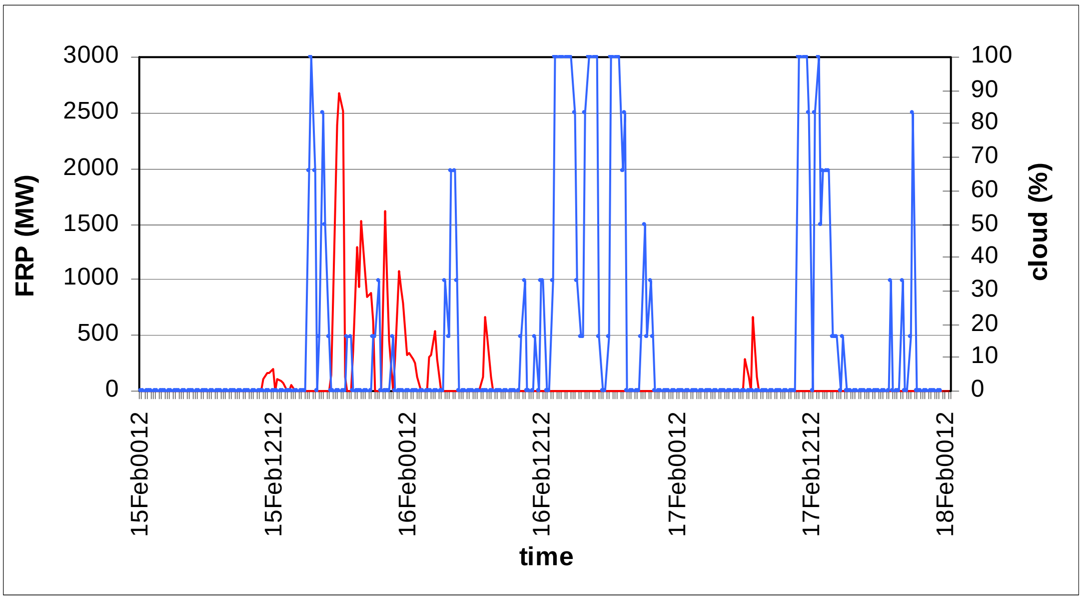

Figure 4.10. Cloud percentage over the fire in Pegli.

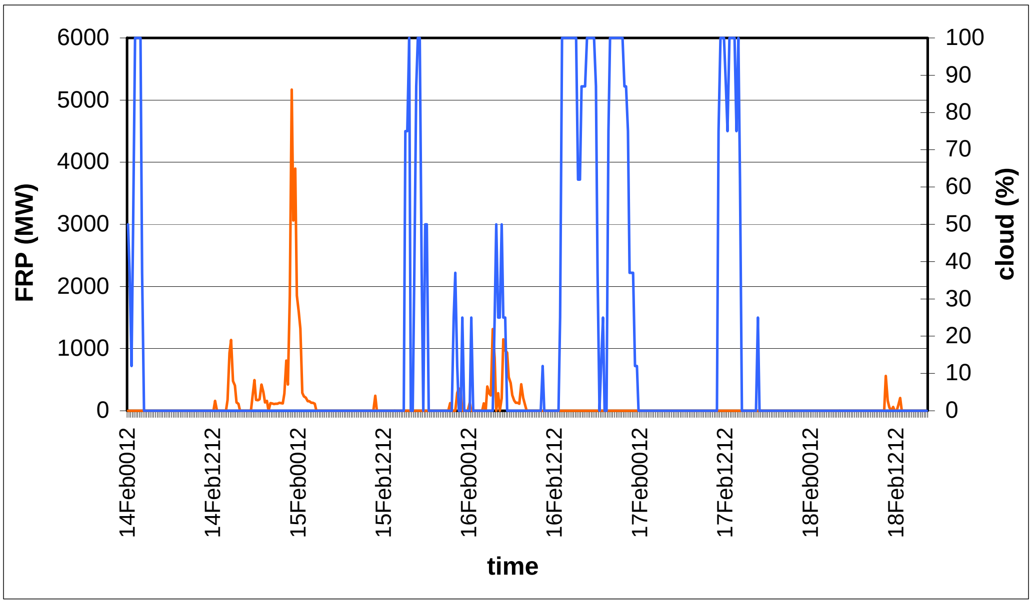

Figure 4.11. Cloud percentage over the fire in Savona.

In order to limit the underestimation of FRP due to cloud cover and the missing images, the FRP time series are interpolated so that the FRP values in the gaps are derived. Interpolation is carried out by using the mean derived from the FRP values before and after the missing data. However in case of a long gap (more than 2 hours of missing data), the average FRP value of the whole time series is used so that the variability of the fire activity is taken into account.

4.2.1. Fire Radiative Energy and burned biomass estimation

The Fire Radiative Energy is derived from the FRP values by temporal integration over time. The radiant energy is considered constant between two acquisitions, therefore the FRE is derived by simple sum up of the FRP values multiplied by the duration of a complete acquisition (15’ · 60’’).

The FRP time series are considered with and without interpolation to provide two estimates of FRE and show the effect of underestimation due to cloud cover. The FRE values are reported in table 4.4. with the corresponding amount of burned biomass which is derived using equation 11. The empirical formula used for the estimation of burned biomass was derived from the field measurements collected in the tropics (Wooster et al., 2005). However there is no evidence that the relation between FRE and the burned biomass depends on the vegetation type, therefore it is used for the case studies in the Mediterranean region.

	Pegli	Sestri L.	Savona
FRE without interpolation (10^6 MJ)	26	24	36
Biomass burned (10^3 ton)	9	8	13
FRE with interpolation (10^6 MJ)	34	26	42
Biomass burned (10^3 ton)	12	10	15

Table 4.4. FRE and burned biomass estimates of the case studies.

The FRE values derived without interpolation of the FRP values show that the fire in Savona reaches the highest level of radiant energy and the biggest amount of burned biomass, whereas the fire of Pegli and Sestri have both lower values of energy and biomass. However if the interpolated FRE are considered, the fires in Pegli and Savona become more similar because of the different cloud cover which affects the sites. The fire in Pegli shows a more persistent cloud cover and the amount of burned biomass is increased by 24% when the FRE values are interpolated, whereas in Savona the increment due to interpolation is about 14%. The FRE of the fire in Sestri is only adjusted for the missing images and the resulting FRE is 11% higher than the original value. The interpolation shows that the cloud cover can have a large impact on the estimation of FRE and therefore it is crucial to take into account this issue when the fire energy is assessed.

4.3. Results from the field campaign

In this Section the intermediate results of the field data analysis are shown. Tree diameters and heights are plotted together in order to derive the relation between the two variables. Most of tree heights were measured in the field, whereas all the tree diameters, within each plot, were measured. Therefore the relation between the heights and diameters is used to determine the tree heights which were not directly measured in the field.

For each sampled plot the best-fit regression function is derived using a logarithmic function type: this is in fact the family of functions which best describes the relation between tree diameters and heights. The statistical analysis is performed using S-PLUS 4 package (1997) which shows that the relations derived for the two variables are statistically significant. The functions are reported in figures 4.12. and 4.13.

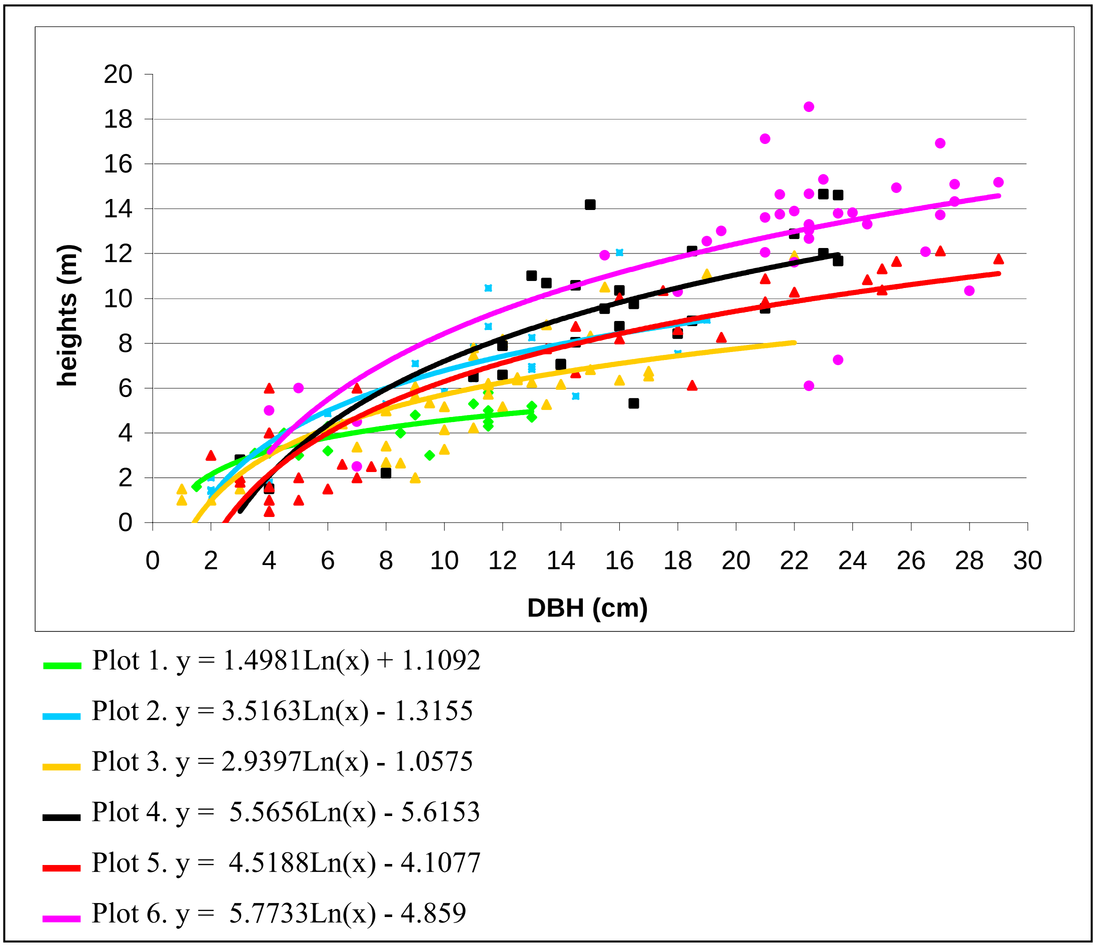

Figure 4.12. Tree heights versus DBH for the six plots in Pegli.

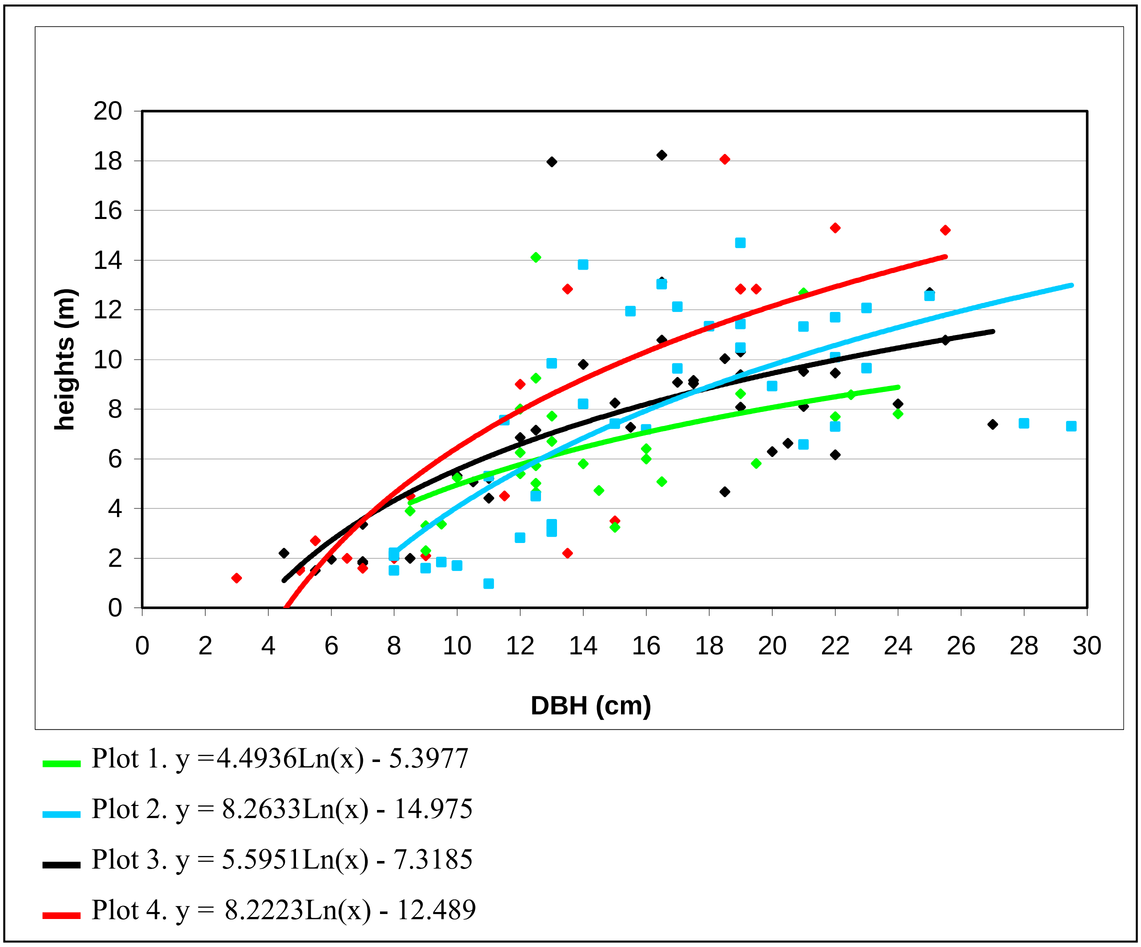

Figure 4.13. Tree height versus DBH for the four plots in Sestri Levante.

The average value of tree basal area is used to determine the mean diameter on each plot; the mean height is derived from the mean diameter using the regression functions shown in the above figures. Information about the sampled forests is reported in table 4.5.

	Pegli			Sestri		
	Tree density (# trees/m^2)	mean DBH (cm)	mean Height (m)	Tree density (# trees/m^2)	mean DBH (cm)	mean Height (m)
Plot 1	0.31	8.1	2.00	0.09	15.5	6.50
Plot 2	0.05	12.0	7.20	0.15	16.5	7.80
Plot 3	0.09	12.0	6.00	0.14	16.5	7.50
Plot 4	0.07	16.0	9.25	0.10	14.5	8.00
Plot 5	0.09	14.5	6.68			
Plot 6	0.07	21.7	13.10			
average	**0.10**	**14.0**	**7.37**	**0.11**	**15.7**	**7.45**

Table 4.5. Forestry data derived for the two case studies.

4.3.1. Biomass estimation

Pre-fire and post-fire biomass volumes are presented in this section. They are derived using information about tree diameters and heights. The regression function used for the pre-fire biomass requires only information about the tree diameter. It provides the dendrometric volume as follows:

$$f = 0.001 \cdot d^2 - 0.0077 \cdot d + 0.0067 \qquad (12)$$

where

d is the tree diameter (DBH).

The post-fire biomass is instead computed using the information on tree diameter and height. The equation estimates the stem volume as follows:

$$f = a \cdot e^{(-0.5 \cdot (((d - x_0)/b)^2 + ((h - y_0)/c)^2))} \qquad (13)$$

where

d is the tree diameter (DBH),

h is the tree height,

x_0, y_0, a, b, c are constants derived with the Sigma Plot Package (x_0 = 56.12, y_0 = 26.98, a = 1.92, b = 19.59, c = 14.29).

The biomass volumes derived for the study areas are reported in table 4.6.

	Pegli			**Sestri**		
	Pre-fire biomass	Post-fire biomass	Burned biomass	Pre-fire biomass	Post-fire biomass	Burned biomass
trees volume over all plots (m^3)	27.80	23.19	4.60	24.09	17.30	6.80
total area of all plots (m^2)	2850			1515		
trees volume (m^3/ha)	97.52	81.38	16.14	159.01	114.16	44.86
trees dry weight (tons/ha)	51.20	42.72	8.48	83.48	59.93	23.55

Table 4.6. Trees volumes and dry weights in the two case studies.

The amount of biomass as dry weight is calculated using the wood density of the tree species. For *Pinus pinaster* the value is equal to 525 kg/m^3 (Giordano, 1981). Finally the difference between the pre and post-fire biomass provides the amount of burned biomass. In Pegli site the tree burned biomass is 8.5 tons per hectare whereas in Sestri L. it is 23.5 tons per hectare which corresponds to about 16% and 28% of the pre-fire tree biomass. The higher consumption rate in Sestri L. is mainly due to the vegetation conditions at the time of burning. Observing the scorched trees on this study site, it is still possible to recognize that many of them were previously affected by *Matsucoccus feytaudi*. This stimulates an extra production of resin along the pine trunk which makes it particularly flammable.

The estimate of the understorey burned biomass is derived combining the data from Viegas (1989) with the observations made in the field campaigns, the values are reported in table 4.7. The amount of fuel load refers to a pure shrubland land cover not mixed with other vegetation types. The original values presented by Viegas are available in a range of variability. Since the understorey is mixed with the pine forest and this confines its vertical growth limiting its biomass load, the lowest values are considered appropriate for the case studies.

	Fuel load (tons/ha)	**Pegli**		**Sestri**	
		Coverage (%)	Burned (%)	Coverage (%)	Burned (%)
Erica arborea	15	41	50	27	45
Arbutus unedo	30	5	30	4	30

Table 4.7. Data used to compute the burned biomass of the understorey in Pegli and Sestri L. sites.

For the study area in Savona the tree biomass burned is derived using the average values of burned biomass in the sampled sites, whereas the understorey is estimated using the mean values of the percentages of burned biomass and the fractional cover from the sampled sites (table 4.8.). This approximation is possible since the area is covered by the same vegetation type and, according to the Italian Forest Service the fire intensity is similar to that of the other case studies.

Savona				
forest		**understorey**		
trees volume (m^3/ha)	30.5		Coverage (%)	Burned (%)
		Erica arborea	34	47
trees dry weight (tons/ha)	16	Arbutus unedo	4.5	30

Table 4.8. Burned biomass estimates for Savona study area.

In order to calculate the total amount of burned biomass the contributions of the forest and the understorey burned biomass are summed up. The cumulative burned biomass of all the plots is normalized over the total sampled area (i.e. the area covered by all the plots) in each case study. In this way the final burned biomass estimation is expressed in tonnes per hectares. The whole burned biomass in Pegli study site is $15 \cdot 10^3$ tons, while in Sestri L. it is $12 \cdot 10^3$ tons. Despite the big difference in terms of area burned (the area burned in Pegli is almost three times the area burned in Sestri L.), the two case studies are comparable in terms of burned biomass due to the higher fire intensity which is registered in Sestri Levante. A similar consideration can be made for the study area in Savona: it shows the highest amount of burned biomass although it is not the largest burned area. The values used to determine the burned biomass are derived from the other case studies and applied to the whole burned area (950 ha). Since the average burned biomass is considered, the total burned biomass is higher than the value in Pegli, although its burned area is smaller. The total amounts of burned biomass for the three case studies are shown in table 4.9.

	Pegli	**Sestri**	**Savona**
Forest burned biomass (10^3 tons)	13	12	15
Understorey burned biomass (10^3 tons)	1.9	0.4	0.9
Total burned biomass (10^3 tons)	**15**	**12**	**16**

Table 4.9. Totals of burned biomass on the three case studies.

4.4. Comparisons of burned biomass estimates

The amounts of burned biomass derived from the FRE are compared with the field data considering both the original FRE and the FRE derived through interpolation of the FRP time series. The field-based estimates have a level of accuracy of 10-20% and are used as a reference.

In general the amount of burned biomass derived from the FRE is underestimated when compared to the field reference. This is due to several causes: the missing detections of the active fires, the cloud cover which obscures the fires, the atmospheric attenuation which can reduce the signal and the interception of the radiant energy by the tree canopy (Roberts et al., 2005).

The causes of underestimation relevant to the analysed case studies are: the fire detection algorithm and the interpolation method used to derive the missing FRP values.

The FRE estimates lay in a range of variability which depends on the uncertainty attached to the values. The uncertainty of the FRE is mainly due to the fire detection algorithm: if the algorithm introduces an omission error, the FRE is not derived and the total value is underestimated. The uncertainty due to the fire detection algorithm is therefore a major cause of underestimation and it is estimated to be around 15%. Therefore the provided FRE value could be increased up to 15%.

The interpolation method used to derive the missing FRP values has also an effect on the FRE estimates. The FRE can vary of ±8% depending on the interpolation method which is applied. The range of variability is derived from the comparison of a set of FRE computed with different interpolation methods.

The uncertainties described above are independent from each other and therefore can be combined together to derive the overall uncertainty in the FRE estimates. Since the fire detection algorithm contributes only to the underestimation of the FRE, the lower limit in the uncertainty range depends only on the interpolation method used. The uncertainty therefore is -8%. The upper limit of the uncertainty range is derived from the combination of the uncertainty due to the fire detection algorithm (15%) and to the interpolation method (8%) according to the following expression:

$$\sqrt{8^2 + 15^2} = 17 \qquad (14)$$

The final level of uncertainty in the FRE estimates varies between -8 and 17%. Such uncertainty affects also the estimates of burned biomass derived from the FRE and it has to be taken into account when the comparison with the field data is carried out. The burned biomass estimates derived from the FRE and from the field are reported in table 4.10. with the corresponding ranges of uncertainty.

Source of burned biomass	Pegli	Sestri	Savona	Uncertainty (%)
Field (10^3 tons)	13 - 18	10 - 14	14 – 19	[-15, +15]
FRE (no interp.) (10^3 tons)	9 - 11	9 - 10	13 – 15	+15
FRE (interp.) (10^3 tons)	11 - 15	10 - 13	14 – 18	[-8, +17]

Table 4.10. Biomass burned derived from the FRE (with and without interpolation) and from the field measurements. The uncertainties associated to each estimate are shown.

The estimates of the burned biomass for each case study are also shown in the figure 4.14. The values lay in a range of variability which depends on the uncertainty of the method applied to derive them. According to the intervals plotted in the figure the ranges clearly overlap with the estimates from the field. Better agreement with the field information is observed in the estimates from the FRE which have been interpolated.

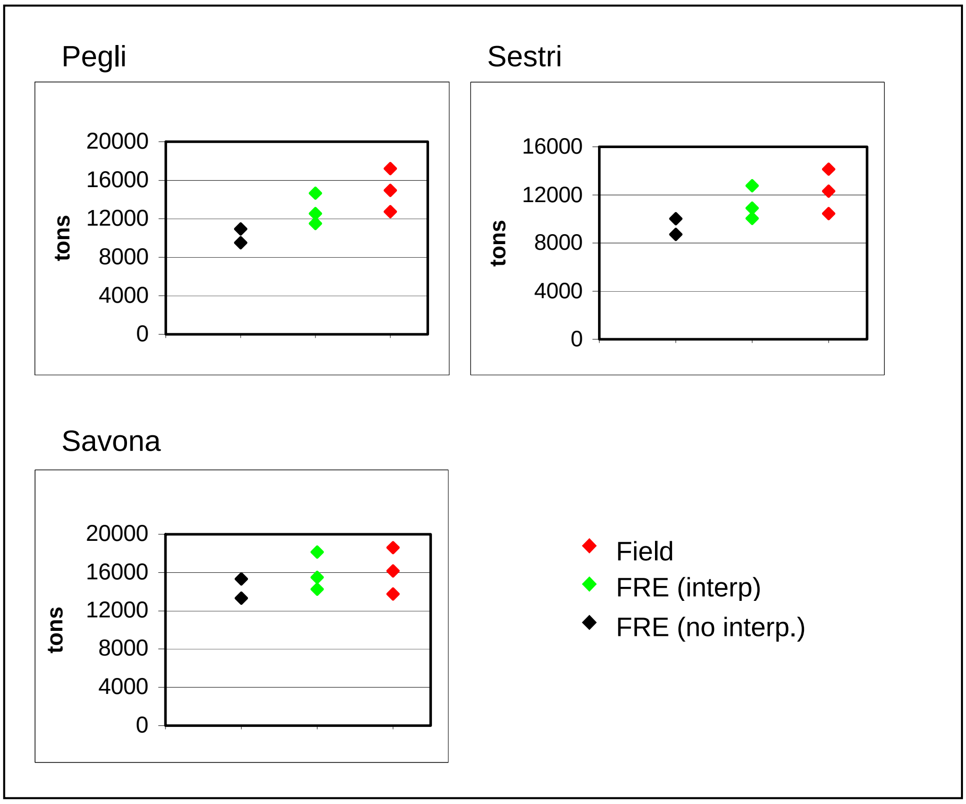

Figure 4.14. Comparison of burned biomass estimates using the field data and the FRE (with and without interpolation). Values are reported with a range of variability due to uncertainty.

The differences between the estimates of burned biomass from the FRE and those from the field are computed considering the uncertainty levels which affect them. The upper and lower limits of uncertainty are applied to the estimates so that they are compared considering both the low limit and the high limit of the possible interval of values. The results of the comparison are reported in table 4.11.

The site of Pegli shows the highest underestimation of FRE: between -36 and -25% when the FRE is considered without interpolation. However when the missing values are interpolated to adjust the time series for the presence of clouds, the underestimation is considerably reduced and the differences with the field data vary between -15 and -9%.

In Savona the underestimation of the burned biomass varies between -18 and -3% when the FRE estimates are considered without interpolation. When the interpolation is applied the FRE estimates are much similar to the field-based results: differences are within -3 and 4% and this indicates the importance of considering the effect of clouds when the FRE approach is applied. Both the sites of Pegli and Savona show about 20% of their FRP time series affected by more than 40% of cloud cover. Therefore when the FRE values are adjusted for the presence of clouds the underestimation shows a strong decrease.

In Sestri Levante the underestimation without interpolation is in the range of -29 and -17% and is improved to values between -10 and -4% when the FRE values are interpolated for the missing images.

Comparison	Pegli	Sestri	Savona
FRE (no interp.) VS field	[-36, -25]	[-29, -17]	[-18, -3]
FRE (interp.) VS field	[-15, -9]	[-10, -4]	[-3, +4]

Table 4.11. Differences between the estimates of burned biomass derived from the FRE (with and without interpolation) and the field reference.

4.5. Emissions estimation

The main greenhouse gases are considered in the analysis. They are: CO_2, CO, CH_4, NO_x and other C-based species. These compounds are the most relevant to climate change. The particular matter is also taken into account since it has an important role in local air pollution and affects human health.

The emitted gas species are reported in table 4.12. The emission factors are derived from Andreae and Merlet (2001): they refer to the *Extratropical Forest Class* and are shown in brackets for each chemical species.

In order to show the sensitivity of the emission estimates to the information on the burned biomass, each chemical species is derived by using three values of burned biomass: the estimates derived from the field campaigns and the estimates derived from the FRE with and without interpolation.

The emissions of each chemical species lay within a range of values which mostly depends on the uncertainty of the emission factors. The variability in the emission estimates due to the different burned biomass is not very wide because there is a general agreement among the estimates of burned biomass. This is particularly evident when the emissions derived by using the burned biomass from the field are compared to those which use the FRE with the interpolated values.

The main contribution in terms of species emitted comes from the carbon dioxide and carbon monoxide: several thousands of tons are emitted in the analysed fires. Also the other species considered are very important like the methane, for example, which has a greenhouse effect 20 times higher than that of the CO_2.

Emitted Species	Source of burned biomass	Emissions (tons)		
		Pegli	Sestri L.	Savona
CO_2 (10^3) (EF: 1569 ± 131)	Field	22.0-25.0	18.0-21.0	23.0-27.0
	FRE no interp.	14.0-16.0	13.0-15.0	19.0-23.0
	FRE with interp.	18.0-21.0	14.0-17.0	22.0-26.0
CO (10^3) (EF: 107 ± 37)	Field	1.0-2.0	0.9-1.8	1.1-2.3
	FRE no interp.	0.7-1.4	0.6-1.3	0.9-1.9
	FRE with interp.	0.9-1.8	0.7-1.4	1.0-2.0
CH_4 (EF: 4.7 ± 1.9)	Field	42.0-99.0	34.0-81.0	45.0-107.0
	FRE no interp.	27.0-63.0	24.0-58.0	37.0-88.0
	FRE with interp.	35.0-83.0	27.0-65.0	43.0-102.0
NMHC (EF: 5.7 ± 4.6)	Field	16.0-154.0	14.0-127.0	18.0-167.0
	FRE no interp.	10.0-98.0	10.0-90.0	15.0-137.0
	FRE with interp.	14.0-129.0	11.0-101.0	17.0-159.0
NO (EF: 3.0 ± 1.4)	Field	24.0-66.0	20.0-54.0	26.0-71.0
	FRE no interp.	15.0-42.0	14.0-38.0	21.0-59.0
	FRE with interp.	20.0-55.0	16.0-43.0	25.0-68.0
N_2O (EF: 0.26 ± 0.07)	Field	2.8-4.9	2.3-4.0	3.0-5.3
	FRE no interp.	1.8-3.1	1.7-2.9	2.5-4.4
	FRE with interp.	2.3-4.1	1.9-3.2	2.9-5.1
CH_3Cl (EF: 0.050 ± 0.032)	Field	0.3-1.2	0.2-1.0	0.3-1.3
	FRE no interp.	0.2-0.8	0.2-0.7	0.2-1.0
	FRE with interp.	0.2-1.0	0.2-0.8	0.3-1.3
BC (EF: 0.56 ± 0.19)	Field	5.5-11.2	4.5-9.2	5.9-12.1
	FRE no interp.	3.5-7.1	3.2-6.5	4.9-9.9
	FRE with interp.	4.6-9.3	3.6-7.3	5.7-11.6
$PM_{2.5}$ (EF: 13.0 ± 7.0)	Field	89.9-299.5	73.7-245.9	97.0-323.4
	FRE no interp.	57.1-190.3	52.3-174.5	79.9-266.4
	FRE with interp.	75.1-250.4	58.9-196-3	92.9-309.6

Table 4.12. The main GHG and particulate species emitted.

Chapter 5

5. Conclusions

The present work addressed a number of important issues in order to improve the knowledge of current burned biomass and atmospheric emissions from forest fires in the Mediterranean region. The research activity contributed to the following issues:

- the detection of active fires from a geostationary satellite system;
- the fire characterization through the derivation of the Fire Radiative Energy (FRE);
- the quantification of the biomass burned by using a satellite-based approach, FRE;
- the comparison of the burned biomass estimates derived from the FRE with the field-based estimates of burned biomass;
- the estimation of gaseous emissions released during the forest fires.

The analysis of the satellite imagery tested the ability of the SEVIRI geostationary system for fire monitoring. Although the sensor has not been designed for fire monitoring and in spite of its low spatial resolution, it was possible to derive active fire maps with a limited number of false alarms and to monitor the fire activity during its whole duration.

The fire detection algorithm was based on the MIR and the TIR bands since they are particularly sensitive to thermal anomalies. However, in some cases, only the MIR recorded an increase in the brightness temperature whereas the TIR band showed much lower temperatures. These different responses are due to the different sensitivity of the two bands to the thermal anomalies. In such cases the conditions for the fire detection were not fulfilled and an omission error could have been introduced. Therefore, a specific test was applied in the fire detection algorithm to verify if the TIR band showed an abnormal low temperature value when compared to the MIR. When this condition was verified a modified set of thresholds was used to detect the active fires.

Another important issue considered for the fire detection was the solar reflective contribution in the MIR channel. If a pixel had a strong reflectance response in the MIR, this could lead to false alarms; therefore a condition on the BRF in the visible band (0.6μm) was applied. The use of this additional criterion considerably reduced the number of false alarms without increasing the omission errors. Finally the combination of multispectral thresholds and the Contextual Fire Test provided a reliable active fire product and minimized the number of false alarms.

The active fire maps were fundamental for the fire characterization which was performed by computing the Fire Radiative Power (FRP). The retrieval of the instantaneous amount of radiant energy emitted (FRP) was for the first time performed in a Mediterranean ecosystem. The heterogeneity of the landscape and the low spatial resolution of the SEVIRI imagery at the latitude of the study areas were taken into account in the implementation of this method. The FRP time series showed the trends in the fire activity and the differences in terms of radiant energy emitted in each case study. The time series showed also several gaps which could be due either to a natural decrease in the fire activity or to an omission in the fire detection. However the analysis of the time series showed that in most cases the missing detection was caused by the high level of cloud cover. Therefore, the missing FRP values due to cloud cover were derived through interpolation of the time series.

Finally, the total amount of energy emitted, the Fire Radiative Energy (FRE), was derived by temporal integration of the FRP values.

The main factors influencing the final value of the FRE are the following:

- the algorithm used for the fire detection;
- the interpolation method used to derive the missing FRP values.

The first point is particularly relevant since if fire is not detected, the FRP is not derived and therefore the FRE is underestimated. The algorithm for fire detection is a source of omission errors whereas no commission errors were considered to affect the case studies. Therefore the algorithm contributes to the uncertainty of the FRE estimates only in terms of underestimation. In the analysed case studies cloud cover is the major cause of non-detection leading to an underestimation of the FRE estimates of about 15%.

Another factor affecting the FRE accuracy is the interpolation method used to derive the missing FRP values in the time series. Small gaps in the data were filled in by using the average of the values before and after the gap; whereas when cloud cover was persistent for a period of a few hours (large gaps) the missing FRP was derived by using the mean value over the whole time series. Different methods can be applied to interpolate the time series: for example large gaps could be filled in by using the average of the FRP values from a cloud free period having the same duration. The interpolation approach used can affect the FRE estimate of about ±8%.

Finally the combination of the two uncertainties led to a variability in the FRE estimates ranging from -8% to 17%. This uncertainty also affects the estimates of the burned biomass which were directly derived from the FRE.

The satellite estimates of burned biomass were compared for the first time with the information derived from the field. The field-based data have a level of uncertainty ranging between 10-20% and were used as a reference to evaluate the accuracy of the estimates derived from the FRE.

The estimates of the burned biomass were also dependent on the equation used to convert the FRE into burned biomass. Since the relation was derived from previous studies which considered spectral field measurements and a different type of vegetation a relation calibrated on the case studies would improve the accuracy of the burned biomass estimates.

In spite of the mentioned uncertainties the agreement between the estimates derived from the FRE and those from the field data is good since their differences vary between 36% and 3%. This is a promising result since the uncertainty attached to current inventories of burned biomass is around 50%.

The derived estimates of burned biomass were used to quantify the greenhouse gases released in the three fire events. The main greenhouse gas species were considered: CO_2, CO, CH_4, NMHCs, CH_3Cl and NO_x together with the more important particulate matters: black carbon and $PM_{2.5}$. These species are relevant for the impacts on the atmosphere and the climate. Moreover the particulate matter affects human health and contributes to local air pollution.

The results of this research activity showed the feasibility of using the SEVIRI geostationary sensor for the assessment of forest fires in a Mediterranean ecosystem. The FRE approach has been proved to be a reliable source of information about the burned biomass and therefore can be used to improve the current estimates of GHG emissions from forest fires and the understandings of their impact on the climate system.

Outlook

Future work can be done on the implementation of the FRE application in the Mediterranean environment. New case studies can be taken into account representing different types of forest and shrubland (e.g. masquis, garrigue).

In the present study the FRP values are integrated over time in order to derive the FRE. The main assumption made in the integration process is that the value of FRP is considered constant between two consecutive acquisitions. However this assumption can be further refined exploring other methods of integration and for example considering a variation in the fire energy between consecutive acquisitions..

The relation between the FRE and the amount of burned biomass can be further analysed using field data from new case studies. This could lead to a refined equation to derive the biomass combusted from the energy estimates and could also improve the accuracy of the burned biomass estimates derived from satellite.

The FRE method has proved to be useful for fire assessment and the burned biomass estimation. However since it is based on the detection of active fires it shows the typical limitations of this approach like: the omissions of fires due to cloud cover or the missing detection of small fires. Therefore it would be useful to integrate other satellite products (i.e. burned area maps) for a more complete assessment of the fire emissions. The information about the extent of the area burned can provide, for example, information about the small fires which are often not detected. In this way the additional use of burned area products can be complementary to the FRP approach and significantly contribute to the analysis of fire emissions.

Another issue which can be considered in future research is the quantification of the indirect emissions caused by forest fires. They are relevant for the effects on the climate change since their emission lasts a much longer period than the direct emissions. They are related to the dead wood and the decomposition processes which start after the fire occurrence. Moreover the carbon which is instead transformed into charcoal should be taken into account as a stable form of carbon not participating in the atmospheric reactions.

Acknowledgements

I would like to thank all the people that, in many ways, contributed to this PhD thesis. First of all I wish to thank my supervisor Professor Valentini who supported my research activity in the last 3 years.

Special thanks go to friends and people of the Inforest Action at the Joint Research Centre (JRC-DG European Commission), where I stayed for almost two years. I thank Jesus San-Miguel who hosted me and gave me the possibility to work within the Action. I spent this period in a very pleasant atmosphere and I would like to thank the many people who gave me valuable suggestions and feedbacks for the work, and great support and fun during my stay.

In particular I wish to thank Paulo, Peter, Annemarie and Tracy who read my thesis and helped with useful comments and brainstorming. All the friends who participated to my work: Jan and Marco for the great support in the programming part and in many other things. Bruna, Lucia and Vicky for the wise advices and Steffen for the special support since the beginning of this experience.

I also want to thank Wolfgang and Vicky for the great time during the field campaigns and the Corpo Forestale (Genova) for the help in accessing the study sites. Finally, I thank my family for the patient support since ever.

Bibliography

Aminou, D. M. A., Jacquet, B., Pasternak, F., 1997. Characteristics of the Meteosat second generation radiometer/imager: SEVIRI, in Proceedings of SPIE Europto Series, vol. 3221, pp. 19– 31, SPIE, Bellingham, Wash.

Andreae, M.O., 1991. Biomass Burning: Its History, use, and distribution and its impact on environmental quality and global climate, in Global Biomass Burning, atmospheric, climatic and Biospheric Implications (Levine ed.), MIT Press, Cambridge, Mass., pp.3-21.

Anderson, J., Ball, J., Bourke, I.J., Braatz, S., Clément, J., Dembner, S.A., Morell, M., Palmberg-Lerche, C., Serrano, O., Warner K., 1999. Unasylva. Mediterranean Forests: An international journal of forestry and forest industries. FAO Food and Agriculture Organization of the United Nations, Editor: S.A. Dembner Editorial Advisory Board Forestry Department. No. 197 -Vol. 50.

Andreae, M. O., J. Fishman, and Lindesay, J., 1996. The Southern Tropical Atlantic Region Experiment (STARE): Transport and Atmospheric Chemistry near the Equator-Atlantic (TRACE A) and Southern African Fire-Atmosphere Research Initiative (SAFARI): An introduction. J. Geophys. Res., 101, 23,519– 23,520.

Andreae M. O., and Merlet, P., 2001. Emission of trace gases and aerosols from biomass burning. Global Biogeochemical Cycles, vol. 15, no. 4, pages 955–966.

Anyamba, A., Justice, C. O., Tucker, C. J., Mahoney, R., 2003. Seasonal to interannual variability of vegetation and fires at SAFARI 2000 sites inferred from advanced very high resolution radiometer time series data. J. Geophys. Res.Vol. 108, No. D13, 8507.

APAT, 2000. Dati su Liguria, Manuali e linee guida 28/2003. Materiale di propagazione forestale e conservazione della biodiversità - Il caso studio della Liguria.

Arino, O., Simon, M., Piccolini, I. and Rosaz, J.M., 2001. The ERS-2 ATSR-2 World Burnt Surface Atlas projects, Proceedings of the 8th ISPRS conference on Physical Measurements and Signatures in Remote Sensing, Aussois, 8-12 January 2001.

Bagnaresi, U., Bernetti, G., Cantiani, M., Hellrigl, B., 1987. Nuove metodologie nella elaborazione dei piani di assestamento dei boschi. ISEA. Bologna.

Barbosa, P.M., Pereira, J.M.C. and Grégoire, J.-M., 1998. Compositing Criteria for Burned Area Assessment Using Multitemporal Low Resolution Satellite Data. Remote Sensing of Environment, 65, 38-49.

Benassi, L. ISAFA, 1970. L'Italia forestale e montana, pag. 157, Firenze, 1946.

Buermann, W., Anderson, B., Tucker, C. J., Dickinson, R.E., Lucht, W., Potter, C., S., Myneni, R. B., 2003. Interannual covariability in Northern Hemisphere air temperatures and greenness associated with El Niño-Southern Oscillation and the Arctic Oscillation. J. Geophys. Res.Vol. 108, No. D13, 4396.

Cofer, W. R., Levine, J. S., Sebacher, D. I., Winstead, E. L., Riggan, P. J., Stocks, B. J., Brass, J. A., Ambrosia, V. G. and Boston, P. J., 1989. Trace gas emissions from chaparral and boreal forest fuels. J. Geophys. Res., 94, pp. 2255– 2259.

Conard, S. G., and G. A. Ivanova, 1997. Wildfire in Russian boreal forests: Potential impacts of fire regime characteristics on emissions and global carbon balance estimates. Environ. Pollut., 98(3), 305–313.

Conard, S. G., Sukhinin, A. I., Stocks, B. J., Cahoon, D. R., Davidenko, E. P. , and Ivanova, G. A., 2002. Determining effects of area burned and fire severity on carbon cycling and emissions in Siberia. Clim. Change, 55(1–2), 197–211.

Crutzen, P. J., and M. O. Andreae, 1990. Biomass burning in the tropics: Impact on atmospheric chemistry and biogeochemical cycles, Science, 250, 1669– 1678.

DeBano L., F., Neary, D., G., Ffolliott, P., F.,1998. Fire's Effects on Ecosystems. J. Wiley and Sons, Inc.

Deering, D. W., 1989. Field measurements of bidirectional reflectance, in Theory and Applications of Optical Remote Sensing (G. Asrar, Ed.), Wiley, New York, pp. 14-61.

Delmas R.A., A. Druilhet, B. Cros, P. Durand, C. Delon, J.P. Lacaux, J.M. Brustet, D. Serça, C. Affre, A. Guenther, J. Greenberg, W. Baugh, P. Harley, L. Klinger, P. Ginoux, G. Brasseur, J.M. Gregoire, P. Barbosa, E. Janodet, A. Tournier, B. Glenat, P.E. Perros, T. Marion, A. Gaudichet, H. Cachier, S. Ruellan, P. Masclet, S. Cautenet, D. Poulet, C. Bouka Biona, D. Nganga, J.P. Tathy, A. Minga, J.

Loemba Ndembi, J.M. Pereira, P.A. Brivio, P. Ceccato, C. Nielsen, 1999. Experiment for Regional Sources and Sinks of Oxidants (EXPRESSO): An overview, Journal of Geophysical Research, 104, 30 609-30 624.

Doreen S. B and F. Petitcolin, 2004. Remote sensing of the terrestrial environment using middle infrared radiation (3.0-5.0 μm). Int. J. Remote Sensing, Vol. 25, No. 17, pp. 3343-3368.

Dozier, J., 1981. A Method for satellite identification of surface temperature fields of sub-pixel resolution. Remote Sensing of Environment, 11,221-229.

Dignon, J., and J.E. Penner, 1991. Biomass burning: A source of nitrogen oxides in the atmosphere, in Global Biomass Burning, ed. by J. Levine, MIT press, Cambridge, MA, 370-375.

Dignon J., 1988. Time and spatially dependent estimates of pollutant trace gas emissions and their effect on tropospheric ozone. Doctoral Dissertation, State University of New York at Stony Brook, Stony Brook NY.

Drouin, A.; Karcher, F., 2003. Systematic errors of total ozone retrievals using the 9.7-micron channel Earth radiance J. Geophys. Res.Vol. 108, No. D13, 4397.

Dwyer E., Gregoire, J.-M., Malingreau, J.-P., 1998. A Global Analysis of Vegetation Fires using Satellite Images: Spatial and Temporal Dynamics. Ambio, 27:75-181.

Elias, T., Piketh, S., J., Burger, R., Silva, A., 2003. Exploring the potential of combining column-integrated atmospheric polarization with airborne in situ size distribution measurements for the retrieval of an aerosol model: A case study of a biomass burning plume during SAFARI 2000. J. Geophys. Res.Vol. 108, No. D13, 8508.

Eva, H. and E. Lambin, 1998. Remote sensing of biomass burning in tropical regions: sampling issues and multisensor approach, Remote Sening of Environment., 64, 292-315.

Eva, H., and Flasse, S., 1996. Contextual and multiple-threshold algorithms for regional active fire detection with AVHRR data. Remote Sensing of Environment, 14: 333-351.

Eva, H., Lambin, E.F., 1998. Burned area mapping in Central Africa using ATSR data. International Journal of Remote Sensing, 9, 3473-3497.

European Commission - Joint Research Centre. Image 2000 and CLC 2000. Products and Methods. EUR 21757 EN © European Communities 2005.

European Commission - Joint Research Centre. Forest Fires in Europe 2005. EUR 22312 EN © European Communities 2006.
http://effis.jrc.it/documents/2006/ForestFiresInEurope2005.pdf

FAO, 2006. Global Forest Resources Assessment 2005, Main Report. Progress Towards Sustainable Forest Management. FAO Forestry Paper 147. Rome.

FAO, 1998. World Reference Base for Soil Resources. World Soils Report No. 84, 88pp. Roma.

FCCC/ARR/2005/PRT. Report of the individual review of the greenhouse gas inventory of Portugal submitted in 2005.

FIRESCAN Science Team, 1996. Fire in Ecosystems of Boreal Eurasia: The Boreal Forest Island Fire Experiment Fire Research Campaign Asia-North (FIRESCAN), in Biomass Burning and Global Change, edited by J. S. Levine et al., pp. 848– 873, MIT Press, Cambridge, Mass.

Fishman, J., Hoell, J. M., Bendura, R. D., McNeil, R. J. and Kirchhoff, V. W. J. H., 1996. NASA GTE TRACE-A Experiment (September-October 1992): Overview. J. Geophys. Res., 101, 23,865–23,879.

Flannigan, M.D., and Vonder Haar, T.H., 1986. Forest fire monitoring using NOAA satellite AVHRR, Canadian Journal of Forest Resources, 16, 975-982.

Flasse, S. P., Ceccato, P., 1996. A contextual Algorithm for AVHRR Fire detection. International Journal of Remote Sensing 17, 419-424.

Food and Agriculture Organization of the United Nations (FAO), 2001. FRA Global Forest Fire Assessment 1990-2000. Forest Resources Assessment Programme, Working Paper 55, p. 189-191. FAO, Rome, 495 p.
http://www.fao.org.0/forestry/fo/fra/docs/Wp55_eng.pdf

French, N. H., Goovaerts, P., Kasischke, E. S., 2004. Uncertainty in estimating carbon emissions from boreal forest fires, Journal of Geophysical Research 109, D14S08.

Goudsblom, J., 1992. Fire and Civilization. Allen Lane. The Penguin Press, New York.

Giglio, L., J. D. Kendall, and R. Mack, 2003a. A multi-year active fire data set for the tropics derived from TRMM VIRS, Int. J. Remote Sens., 24, 4505–4525.

Giglio, L., Descloitres, J., Justice C.O., Kaufman, Y. J., 2003b. An Enhanced Contextual Fire Detection Algorithm for MODIS. Remote Sensing of Environment, Vol. 87 pp. 273–282.

Giordano, G., 1981. Tecnologia del legno – Vol. I "La materia prima", UTET.

International Forest Fire News (IFFN) No. 29 (July – December 2003, 40-55). Outcomes of the International Wildland Fire Summit. Sydney, Australia, 8 October 2003. http://www.fao.org/forestry/webview/media?mediaId=6990&langId=1.

International Union for the Conservation of Nature and Natural Resources (IUCN) and World Wildlife Fund (WWF). Background Information. Forest fires in the Mediterranean. http://iucn.org/places/medoffice/documentos/Background_med_forest_fires.pdf.

Jarvis, A., H., I., Reuter, A., and E. Guevara, 2006. Hole-filled seamless SRTM data V3. International Center for Tropical Agriculture (CIAT) http://srtm.csi.cgiar.org/.

Justice C.O., and Dowty, P., 1994. IGBP-DIS Satellite fire detection algorithm workshop technical report. IGBP-DIS working paper, 9, 88pp. February 1993, NASA/GSFC, Greenbelt, Maryland, USA.

Justice C.O., Malingreau J-P, Setzer AW., 1993. Satellite remote sensing of fires: potential and limitation. In: Crutzen PJ, Goldammer JG (eds). Fire in the environment: the ecological, atmospheric and climatic importance of vegetation fires. John Wiley and Sons, New York, pp 77-88

Justice, C., and Malingreau, J.P., 1996. Report of the IGBP-DIS Fire Algorithm Workshop, IGBP-DIS Working Paper 14, Ispra, Italy.

Kasischke, E. S., N. L. Christensen Jr., and B. J. Stocks, 1995. Fire, global warming, and the carbon balance of boreal forests, Ecol. Appl., 5, 437– 451.

Kaufman, Y.J., Remer, L., Ottmar, R., Ward, D.,Rong-R., L., Kleidman, R. G., Fraser, R., Flynn, L., McDougal, D., Shelton, G., 1996. Relationship between remotely sensed fire intensity and rate of emission of smoke: SCAR-C experiment, in Levine (Ed.). Global Biomass Burning (Cambridge, MA: MIT Press), 685-696.

Kaufman, Y. J., Hobbs, P. V., Kirchhoff, V. W. J. H., Artaxo, P., Remer, L. A., Holben, B. N., King, M. D., Prins, E. M., Ward, D. E., Longo, K. M., Mattos, L. F., Nobre, C. A., Spinhirne, J. D., Ji, Q., Thompson, A. M., Gleason, J. F., Christopher, S. A., & Tsay, S.-C., 1998a. Smoke, Clouds, and Radiation – Brazil (SCAR-B) experiment. Journal of Geophysical Research 103, 31,783–31, 808.

Kaufman, Y.J., Kleidman, R.G., King, M.D., 1998b. SCAR-B fires in the tropics: Properties and remote sensing from EOS-MODIS. Journal of Geophysical Research 103, 31,955-31,968.

Kaufman Y.J., Justice C.O., Flynn L.P., Kendall J.D., Prins E.M., Giglio L., Ward D.E., Menzel W.P., Setzer A.W., 1998c. Potential global fire monitoring from EOS-MODIS. Journal of Geophysical Research-Atmospheres. Vol 103, Iss D24, pp 32,215-32,238.

Langaas, S., 1995. A critical review of sub-resolution fire detection techniques and principles using thermal satellite data. Ph.D. thesis, Dep. of Geography. University of Oslo. Norway.

Levine, J. S., 1991. Global Biomass Burning: Atmospheric, Climatic, and Biospheric Implications, Levine Ed. The MIT Press: Cambridge, MA.

Levine, J.S., Cofer, W., R., Cahoon, D., R., JR., Winstead, A.L., 1995. Environmental Science and Technology. The Global Impact of Biomass Burning.
http://asd-www.larc.nasa.gov/biomass_burn/globe_impact.html.

Levine, J.S. (ed.), 1996. Biomass Burning and Global Change, MIT Press, Cambridge, Mass.

Levine, J.S., Cofer, W.R., 2000. Boreal forest fire emissions and the chemistry of the atmosphere. In: Kasischke, Eric S.; Stocks, Brian J., eds. Fire, Climate Change, And Carbon Cycling In The Boreal Forest. Ecological Studies Vol. 138. New York: Springer-Verlag: 31-48.

Li, Z., Kaufman, Y.J., Ichoku, C., Fraser, R., Trishchenko, A., Giglio, L., Jin, J., Yu, X., 2000. A Review of AVHRR-based Active Fire Detection Algorithms: Principles, Limitations, and Recommendations. In: Forest Fire Monitoring and Mapping: A Component of Global Observation of Forest Cover. Editors: Ahern, Gregoire and Justice, Ispra, Italy, 3-5 November 1999.

Z. Li, S. Nadon and J. Cihlar, 2000. Satellite-based detection of Canadian boreal forest fires: development and application of the algorithm Int. J. Remote Sensing. Vol. 21, no. 16, pp. 3057–3069.

Lillesand, T.M., and Kiefer, R.W., 2000. Remote Sensing and Image Interpretation. Copyright © 2000 John Wiley & Sons, Inc.

Lindesay, J. A., M. O. Andreae, J. G. Goldammer, G. Harris, H. J. Annegarn, M. Garstang, R. J. Scholes, and B. W. van Wilgen, 1996. International Geosphere-Biosphere Programme/International Global Atmospheric Chemistry SAFARI 92 field experiment: Background and overview. J. Geophys. Res., 101, 23,521–23,530.

Lobert, J. M., D. H. Scharffe, W. M. Hao, T. A. Kuhlbusch, R.Seuwen, P. Warnesk, and P. J. Crutzen, 1991. Experimental evaluation of biomass burning emissions: Nitrogen and carbon containing compounds. In J. S Levine (ed.), Global Biomass Burning: Atmospheric, Climatic, and Biospheric Implications. MIT Press, Cambridge, Mass., pp.289-304.

Lobert J.M., Warnatz, J., 1993. Emissions from the combustion process in vegetation. Fire in the Environment: The Ecological, Atmospheric and Climatic Importance of Vegetation Fires. Crutzen, P.J. and Goldammer, J.G., (Eds.). (New York: John Wiley and Sons), 15-39.

Malingreau, J.P., 1990. The contribution of Remote Sensing to the Global Monitoring of Fires in Tropical and Subtropical Ecosystem, in Fire in the Tropical Biota. Ecosystem Processes and Global Challenges, (Goldammer Ed.), Ecological Studies, 84, Springer-Verlag, Berlin, 15:337-368.

Manson, A. H.; Meek, C. E.; Avery, S. K.; Thorsen, D., 2003. Ionospheric and dynamical characteristics of the mesosphere-lower thermosphere region over Platteville (40°N, 105°W) and comparisons with the region over Saskatoon (52°N, 107°W). J. Geophys. Res.Vol. 108, No. D13, 4398.

Martin, M.P., Ceccato, P., Flasse, S. and Downey, I., 2003. Fire detection and fire growth monitoring using satellite data. In Wildland fire danger estimation and mapping: The Role of Remote Sensing Data. Edited by Chuvieco. E.S. River Edge, N.J. World Scientific, pp. 101-122.

Meschini A. ISAFA, 1970. Piano di assestamento decennio 1960-1969.

Miranda, A. I., Coutinho, M. and Borrego, C., 1994. Forest fire emissions in Portugal: A contribution to global warming? Environmental Pollution. Volume 83, Issues 1-2 , 1994, Pp. 121-123.

Mouillot, F., Ratte, J.P., Joffre, R., Moreno, J.M., Rambal, S., 2003. Some determinants of the spatio-temporal fire cycle in a mediterranean landscape (Corsica, France). Landscape Ecology, 18, 665-674.

Myneni R. B., and G. Asrart, 1994. Atmospheric Effects and Spectral Vegetation Indices. Remote Sensing of Environment: 47:390-402.

Pereira J.M.C., Ana, C.L. Sà, Adélia M.O. Sousa, Silva, J.M.N., 2003. Spectral characterization and discrimination of burned areas. In Wildland fire danger estimation and mapping: The Role of Remote Sensing Data. Edited by Chuvieco. E.S. River Edge, N.J. World Scientific, pp.123-138.

Piñol J, Terradas, J. and Lloret, F., 1998. Climate warming, wildfire hazard, and wildfire occurrence in coastal eastern Spain. Climatic Change, 38, pp 345-357.

Pozo D., Olmo, F.J., Alados Arboledas, L., 1997. Fire Detection and growth monitoring using a multitemporal technique on AVHRR mid-infrared and thermal channels. Remote Sensing of Environment 60, 111-120.

Queface, A. J., Piketh, S., J., Annegarn, H. J., Holben, B.,N., Uthui, R., J., 2003. Retrieval of aerosol optical thickness and size distribution from the CIMEL Sun photometer over Inhaca Island, Mozambique. J. Geophys. Res.Vol. 108, No. D13, 8509.

Roberts, G., Wooster, M. J., Perry, G. L. W., Drake, N., Rebelo,, L. M., Dipotso, F., 2005. Retrieval of biomass combustion rates and totals from fire radiative power observations: Application to southern Africa using geostationary SEVIRI imagery, J. Geophys. Res., 110, D21111.

Robinson, J.M. 1991. Fire from space. Global fire evaluation using infrared remote sensing. International Journal of Remote Sensing. Vol. 12, no. 1, pp. 3-24.

S-PLUS 4 Guide to Statistics, 1997. Data Analysis Products Division, MathSoft, Seattle.

Saunders, R. W., and K. T. Kriebel, 1988. An improved method for detecting clear sky and cloudy radiances from AVHRR data, Int. J. Remote Sens., 9, 123– 150.

Schimel, D.S. 1995. Terrestrial ecosystems and the global carbon cycle. Global Change Biology. 1: 77–71.

Schlesinger, W., H., 1991. Biogeochemistry: An analysis of Global Change, Academic Press, San Diego.

Seiler, W., Crutzen, P.J., 1980. Estimates of gross and net fluxes of carbon between the biosphere and the atmosphere from biomass burning. Climate Change, 2, 207-247.

Simon, M., S. Plummer, F. Fierens, J. J. Hoeltzemann and O. Arino, O., 2004. Burnt area detection at global scale using ATSR-2: the GlobScar products and their qualification, Journal of Geophysical Research, 109, D14, D14S02.

Stocks, B. J., and J. B. Kauffman, 1997, Biomass consumption and behavior of wildland fires in boreal, temperate, and tropical ecosystems: Parameters necessary to interpret historic fire regimes and future fire scenarios, in Sediment Records of Biomass Burning and Global Change, NATO ASI Ser. 1, vol. 51, edited by J. S. Clark et al., pp. 169–188, Springer-Verlag, New York.

Swap, R. J., Annegarn, H. J., Suttles, J. T., King, M. D., Platnick, S., Privette, J., L., Scholes, R. J., 2003. Africa burning: A thematic analysis of the Southern African Regional Science Initiative (SAFARI 2000). J. Geophys. Res.Vol. 108, No. D13, 8465.

Trollope W.S.W., Trollope, L.A., Potgieter, A.,L.,F. and Zambatis, N., 1996. SAFARI-92 characterization of biomass and fire behaviour in the small experiment burns in Kruger National Park. Journal of Geophysical Research, 101, 23, 531-23,540.

Viegas, D., 1989. Manual sobre Incêndios Florestais; Secretaria-Geral do Ministério do Planeamento e da Administração do Território, Lisboa.

West P.W., 2004. Tree and Forest Measurements. Springer-Verlag Editors, pp. 1-165.

Whelan R.J., 1995. The Ecology of Fire, Cambridge Uninversity Press, New York.

Wooster, M.J., 2002. Small-scale experimental testing of fire radiative energy for quantifying mass combusted in natural vegetation fires, Geophysical Research Letters, 29(21) 2027.

Wooster, M.J., Zhukov, B., Oertel, D., 2003. Fire radiative energy for quantitative study of biomass burning: Derivation from the BIRD experimental satellite and comparison to MODIS fire products, Remote Sens. Environ., 86, 83–107.

Wooster, M.J. and Roberts, G. MTG Final Report: Review of MTG FDHSI Mission Requirements Regarding Fire Applications. EUM/PPS/SOW/04/0055. June 2004.

Wooster, M. J., Perry, G., Zukov, B., Oertel, D., 2004. Biomass burning emissions inventories: Modelling and remote sensing of fire intensity and biomass combustion rates, in Spatial Modelling of the Terrestrial Environment, edited by R. Kelly, N. Drake, and S. Barr, pp. 175–196, John Wiley, Hoboken, N. J.

Wooster, M. J., Roberts, G., Perry, G. L. W., 2005. Retrieval of biomass combustion rates and totals from fire radiative power observations: FRP derivational and calibration relationships between biomass consumption and fire Radiative Energy Release, J. Geophysical Research, Vol 110, D24311.